Dear Alexander Kokhanovsky,

Please find attached our revised manuscript and responses to referees.

This file contains, besides this page, the author comments we submitted and a “diff-file”, highlighting the changes made to the manuscript. The revised manuscript is submitted as a separate file.

Most manuscript changes are done in direct response to referee comments. These are discussed on the following pages and are not repeated here. Beside pure language corrections, the other additional changes are:

- In Sec 2.1, A-CDS is changed to ARGOS-4, which is the name that will be used for EPS-SG.

- At the end of the same section, we have added a comment about MWI, as a comment on text added in Sec. 1, following the advice by Ralph Ferraro.

- Sec 2.3, 784 changed to 785, following a recent update made at EUMETSAT.

- DOI for Mattioli et al. added.

Kind regards,

Patrick Eriksson and co-authors

Atmos. Meas. Tech. Discuss.,
doi:10.5194/amt-2019-312-AC1, 2019

Atmospheric Measurement Techniques Discussions

Interactive comment on "Towards an operational Ice Cloud Imager (ICI) retrieval product" *by* Patrick Eriksson et al.

Patrick Eriksson et al.

patrick.eriksson@chalmers.se

Received and published: 19 November 2019

Dear Ralph Ferraro,

Thanks for the kind words about our manuscript.

Joint MWI-ICI retrievals are already mentioned in Sec. 5, but we will add a comment on this possibility in Conclusions. We avoid discussing MWS as it will be on the other platform and the time difference between platforms A and B will be relatively high, about 50 min (SG-1B will be positioned at about 180 degrees relative to SG-1A).

All your minor comments will be followed.

Best regards,

C1

Patrick and co-authors

Interactive comment on Atmos. Meas. Tech. Discuss., doi:10.5194/amt-2019-312, 2019.

Atmos. Meas. Tech. Discuss.,
doi:10.5194/amt-2019-312-AC2, 2019

Atmospheric Measurement Techniques Discussions

Interactive comment on "Towards an operational Ice Cloud Imager (ICI) retrieval product" *by* Patrick Eriksson et al.

Patrick Eriksson et al.

patrick.eriksson@chalmers.se

Received and published: 19 November 2019

Dear Stuart Fox,

Thanks for the kind words about our manuscript.

Yes, it is unlucky that we have only a single habit for mid-latitudes and, as you point out, that may give an over-estimation of the retrieval performance. We also write that the mid-latitude results shall be approached with care (page 15, lines 20-21). We will add a clarification that the lack of multiple habits is one reason for the concern. We will also stress this stronger in the Outlook part.

We would like to mention that the efforts so far have focused on the core algorithm and the retrieval database discussed has been produced as an initial working basis. Future

studies will be required to expand the database. Accordingly, it could be produced by persons not involved in the work presented here. We will clarify in the revised manuscript.

We will better explain that RT4 indeed is applied following the independent beam approximation.

Best regards,

Patrick and co-authors

Interactive comment on Atmos. Meas. Tech. Discuss., doi:10.5194/amt-2019-312, 2019.

Atmos. Meas. Tech. Discuss.,
doi:10.5194/amt-2019-312-AC3, 2019

Atmospheric Measurement Techniques Discussions

Interactive comment on "Towards an operational Ice Cloud Imager (ICI) retrieval product" *by* Patrick Eriksson et al.

Patrick Eriksson et al.

patrick.eriksson@chalmers.se

Received and published: 19 November 2019

Thanks for the kind words about our manuscript.

Below we will try to answer your questions and what changes of the manuscript we will implement. Your comments are in italic, with our answers below.

As the retrieval database is in the background of many of the questions, we start by mentioning that the efforts so far have focused on the core algorithm and the retrieval database discussed has been produced has to be considered an initial working basis. Future studies will be required to expand the database.

1. Section 3.4.4: Why are channels masked out if they have any surface contribution? Equation 13 shows the Bayesian uncertainty is increased for channels with surface

contribution, and in a Bayesian context that approach is all that should be needed to deal with the uncertainty of surface emissivity. Won't the varying number of channels included in the retrievals cause spurious (if not statistically significant) discontinuities in the retrievals between pixels with close brightness temperatures? Perhaps some more justifications or caveats are needed in this discussion.

It is correct that the surface term in Eq. 13 and the channel selection to some extent do the same thing. However, Eq. 13 models the uncertainty in a simplistic manner. The main limitation is that the correlation between channels is ignored. An error in assumed surface emissivity will cause an error that is correlated between channels, but presently we have no knowledge at all on this correlation at sub-mm wavelengths. There should be correlation, but it is likely not one between all channels. See further answer to question 4b.

In any case, if found unnecessary the channel selection can be "deactivated" by setting the optical thickness thresholds to some very high value.

We will add comments to make these aspects clearer.

Yes, there is a high risk that there will be discontinuities in the retrieval at e.g. coasts. They will to a large extent dependent on the quality of the final retrieval database. It could be mentioned that many microwave products are ocean-only, due to the problem of modelling land emissivities, but we wanted to at least keep the door open for producing results over land.

2. Section 3.5.1: The quantile retrieval approach requires a substantial number of database cases that match the observations so that the posterior probabilities are high enough. How is this assured? How can we trust the retrieved quantiles, especially at 5% and 95%?

To our best knowledge, there is no manner to set a required number. The general rule is simple: the more the better! This means that the final retrieval database shall

represent as many cases as possible, and to make this easier we have included the possibility to use a prior weights (a_i).

At the end of the outlook section, we make a comment about that machine learning seems to decrease the demand on database size, and that to apply BMCI for combined MWI and ICI retrievals are probably out of the question.

3. Section 3.5.3: Could you mention how the database extraction filtering does not exclude cases which would contribute significantly to the integral and thus bias the result?

Nothing like this is built into the algorithm. It will depend on sensible choices of the configuration parameters. The recommendation is, of course, to use broad ranges for inclusion and that tests should be performed when the final retrieval database is at hand.

4. The end of section 3.5.3 discusses the important issue of very few or no database cases matching an observation. 4a) Do you have a non-arbitrary method for determining when there are too few matching database cases or too wide a range of probabilities for the matching database cases? What specifically are the criteria for increasing the variances in S_0?

There is no automatic method to set the required number of matches. The number shall be set as high as possible considering the size of the final retrieval database.

We don't see a problem if there is a wide a range of probabilities for the matching database cases. On the contrary, if the range is narrow then you have likely not sampled a sufficient broad part of the a priori distribution.

The rules for increasing variances are important, but require quite some space to describe. For this reason, we decided to only refer to Rydberg (2018) regarding this part.

4b) This problem is exacerbated by the Gaussian pdf assumption for the probability of the difference between an observation and the database simulation. Could you con-

sider using a long-tailed probability distribution, which would be justified by systematic errors, such as various modelling errors?

BMCI is more flexible here than OEM (1D-VAR), but BMCI stills assumes that all uncertainties that are covered by S_o approximately follow Gaussian statistics. So on that side the answer is no. On the other hand, in the generation of the database you are not limited to Gaussian assumptions. (We will add text to clarify this) This means that "outlier cases" can be included in the database.

Above we discussed modelling of surface emissivity. In the generation of the database the emissivity can be varied, and if the knowledge is poor the surface emissivity should be given a broad distribution (that does not need to be Gaussian). This is relatively straightforward. The problem is that the correlation between frequencies of emissivity variations also has an impact, and here reasonable assumptions are very hard to formulate before we actually have the ICI data.

5. Section 4.1 (Remapping of data) needs to summarise the numerical experiment performed in addition to discussing the results.

Will be done.

6. Section 4.1: Why is the incidence angle relevant for remapping errors for a homogeneous scene? The brightness temperatures simulated in the database can use the correct zenith angle for each channel, right?

We briefly discussed that in the Outlook section. We will add some text to Sec 4.1 to make this more clear.

7. Section 4.2 (Generation of retrieval database): It would be useful to include some details about the method for generating the retrieval database used in the experiments in this article.

We see Sec. 4.2 as a general discussion. Details of generation of the database used are found in Sec 4.3.1 (that will be somewhat expanded).

8. Section 4.3.1 (Test retrieval database): How many CloudSat profiles were used? Do the CloudSat profiles correspond to the same 15S to 15N region and the same time(August 2015)?

A smaller dataset, compared to the retrieval database, is used in Fig. 7. We will make this clear.

9. Section 4.3.2 (Degrees of freedom): Again, there needs to be some explanation of the method used here. How is DOF calculated? The bit of explanation in the short figure caption is not enough.

A description of how DOF is calculated will be added.

10. Section 4.3.2: 448.0+-1.4 GHz is an upper troposphere water vapour channel in the Tropics and is considerably more sensitive than the 183 and 325 GHz channels, so one doesn't want to give the impression that the three channels for each water vapor absorption line are equivalent. Is the DOF for low IWP and IWV 3 or 4 (I'm having trouble telling from the colour scale)?

It is correct that the 448 GHz transition is stronger than the 183 and 325 GHz ones, and has the potential to provide information at higher altitudes than the two later transitions. Figure 1 supports this. However, the present NEDT values for the 448 GHz front-end are relatively high. We have not performed a dedicated test, but we suspect that the assumed NEDT gives too noisy data for obtaining information from the two innermost 448 GHz channels, for single-footprint retrievals. (NEDT is also high for 325 GHz, and likely 183 GHz dominates the IWV information content in Fig 8.) We will make a small rewording, and leaves the details to a dedicated study on ICI's performance at clear-sky conditions.

The DOF for low IWP and IWV is 4. We will redo the figure with another colour scale.

11. Section 4.3.3 (Overall performance): A description of the method needed. Do the two regions/seasons (tropical and mid-latitude) use different retrieval databases? Is

there a minimum retrieved IWP for including cases in the Zm and Dm retrieval performance graphs?

There is just one single retrieval database. We will clarify how the database is used. Yes, an IWP threshold is applied in Fig. 9. Thanks for spotting this. We will add this information.

12. The brief section 4.3.4 (Test inversions) should be omitted. It references inversion tests with ISMAR data, but without any validation or results, and thus is not very meaningful.

We will follow this advice.

13. Section 5 (Outlook): Do you have ideas for how to include particle orientation in the algorithm? If not too speculative, your ideas would be interesting in this section.

In fact, we have been working on this topic, and the first data and results just appeared in AMTD. So we will gladly write a few words about this.

14. Section 5: Another important extension to mention is including a wider range of particle size distribution variations. Presumably, the variations in Dm vs IWC curves between single beams is larger than between published climatologies. Also, the width of ice particle size distributions is important for relating CloudSat radar reflectivity to IWC for the prior probabilities. This issue might lead to a significant underestimate in the retrieval errors.

Yes, totally correct. The present text does not make this totally clear. We will rewrite.

Best regards,

Patrick and co-authors

Interactive comment on Atmos. Meas. Tech. Discuss., doi:10.5194/amt-2019-312, 2019.

Atmos. Meas. Tech. Discuss.,
doi:10.5194/amt-2019-312-AC4, 2019

Atmospheric Measurement Techniques Discussions

Interactive comment on "Towards an operational Ice Cloud Imager (ICI) retrieval product" *by* Patrick Eriksson et al.

Patrick Eriksson et al.

patrick.eriksson@chalmers.se

Received and published: 19 November 2019

We deliberately tried to keep the manuscript as short as possible, to not let details cause distraction, but we have clearly been too brief in some parts. The other reviewers made similar remarks for some parts. We will expand the manuscript with the aim to make it more easily accessible for a broader audience.

Below we comment on your specific questions and what changes of the manuscript we will implement. Your comments are in italic, with our answers below.

line 19: I am not in the measurements field and have hard time to understand what is the receiver noise temperature and especially the very large values of 600 to 2600K. Maybe a reference could help the reader to find information on this receiver noise

temperature.

We will add a reference for receiver noise temperature. Much lower values can be achieved by cooled receivers, but cryogenic cooling represents a risk and a relatively short life-time. Hence, such techniques can not be used for operational missions.

line 29: It is actually not evident to get this document, I tried the link documentation under www.nwcsaf.org, but did not find any document related to ICI. Anyway, maybe some annexe would help the reader to understand the details of the algorithm or an academic reference.

We are deeply sorry, but the information in the reference is wrong. The mistake will be corrected.

line 10: What is the dimension (unit) of r? Specify it in the text. You could also be explicit on the solid angle by saying that the solid angle is the one of the antenna (I guess). Concerning the cartesian coordinate we have no idea on where is the origin of this cartesian system. Please specify also if the antenna pattern is taken on the ground, or change with altitude and therefore you need to know the cloud extent (information that you do not have). It is not so evident how you concretely compute IWP.

We will clarify.

line 12: dveq is the equivalent volume diameter but equivalent to what? Spherical particles? Specify it in the text.

Will be done.

line 17: the Author call Dm the mean mass size but Delanoe et al. 2014 expressed it as the volume-weighted diameter because it is the 4th moment of the size distribution over the third one. Why did you call it mean mass size? We don't see any mass weighted in the formulae!

As mass is the volume times density, the volume-weighted and mass-weighted are

equal concepts. Or consider equation 3, showing that d_{veq}^3 is directly proportional to mass. This means that d_{veq}^3 in both integrals represent the mass (factors such as density and π cancel out).

line 9: what do you mean by semi-circular?

We mean "close to circular". We will rephrase.

line 23: Last sentence "As the module likely will not be applied, no details are here given". So if you do not give any detail about the clear sky module detection of the algorithm, do we really need this paragraph?

It is described in Rydberg, 2019. We will make this clear.

line 4 (eq. 9): Could you justify why wi is written like an exponential law?

We will add a reference.

line 5: Why only observation uncertainties are taken into account in S0? Can't you add the forward model uncertainties also (due to the miss-knowledge of non retrieve parameters that play in the forward model to compute yi)?

We used the term "observation uncertainty" as the uncertainty of the observation system, thus including the forward model. We will rephrase to be clearer.

line 6: The following sentence is very hard to understand, please rephrase it. "They are not standard, but are introduced to allow tailoring of the retrieval database to the specifics of the retrievals of concern."

Will be done.

line 14 and 16 (eq. 10 and 11): Something is wrong here because $p(x'|y)$ is what we call a probability density function (PDF) in (10), we need to multiply by dx to get a probability. But in (11) $p(xi|y)$ should be a probability but the notation is almost identical to the previous equation (10), and make this 2 equation confusing. Specify somewhere

that $p(xi|y)$ is not a PDF but directly a probability to have $x = xi$.

Correct. Thanks for pointing this out. Will be fixed. (In fact, above Eq 11 it says p_n, that was meant to flag that it is a probability, but we missed to complete this). Eq 8 will also be corrected.

line 2: Why is there only one clear sky in your database? Don't you need to simulate different clear sky at least to take into account the different emissivity, surface temperature that depend of the season and location?

On the database side, the assumption is that we know the true values and there is only one clear-sky simulation to be done. However, it is critical that the database contains cases covering a distribution of emissivities, surface temperatures etc. See further comments in the reply to referee 1. We think the comments we will add in response to referee 1 will make all this clear.

line 7 (and eq. 13): We don't understand why the uncertainty on emissivity take this form, could you explain a bit or give some reference? We don't even know what is $\tau_{e,j}$?

$\tau_{e,j}$ should have been $\tau_{cs,j}$. Sorry, we missed to change this equation when changing nomenclature for expressing optical thicknesses. We will explain the expression for emissivity uncertainty.

line 9 (and eq. 13): I really don't understand why this last term of equation 13, in its present form, could model the uncertainty due to a miss-representation of the scattering in the model! Please explain why in the text or give a reference!

See answer to the next question.

line 10: Why can you assume that the modeling error (scattering) is proportional to the deviation of clear-sky reference simulation? Where does this assumption comes from? Any Reference?

As we understand it, these two questions refer to the same issue. We will add an

explanation.

3.5.3 Database extraction and iterations: OK now I understand a bit more why there is only one clear sky in the database! You should put this paragraph before the paragraph 3.5.2!

The advice will be followed.

line 8: On figure 6 please indicate the units of the color scale

Will be done.

line 18-19: Difficult to understand the following sentence, maybe a figure could help here! "This means that line-of-sights of observations and the corresponding ones after remapping cross at the ellipsoid but deviate at altitudes inside the atmosphere."

We will rephrase.

line 19: what do you mean by unrealistically high? Give some number. (Correct the word spelling also)

We will add some number(s) and correct spelling.

line 22: why around 0.8? Don't you have an exact number or did you make some random choice around 0.8?

First, 0.8 is a "typo", should be 0.9. Let's call this an "educated guess". We will clarify that there is no reference model for land emissivity is at hand. Accordingly, this value is highly uncertain, and this is why we apply high optical thickness thresholds above land (at least 3).

line 24-25: This comparison between ATMS observations and simulations are done over which period? Does it used every observation or is there some filtering? Are you taking into account any specific antenna pattern of the ATMS instrument? How the atmospheric profile and hydrometeors are define? Are you using Cloudsat also? Are

you using the same definition for the microphysical model than for ICI? Please develop in order to help the reader to understand the limit of this statistical comparison!

Except for footprint size and time period used, all is done as for the retrieval database. We will clarify this.

line 29: Please explain how the particle orientation can explain this discrepancy?

Will be done.

line 31: What is GMI? Any reference?

GMI is introduced in the Introduction, bu the acronym will be explained again and a reference will be added.

Table 2: Could you please indicate the habit model explicitly instead of a number referring to another paper from the author.

Will be done (but will require a two-column table).

line 7-8: The degree of freedom is more commonly called DoFS ...

We will change DOF to DoF.

It was clearly a big mistake to not include a description of how we calculate the DoF. Both you and referee 1 ask for it. And by your comments we notice that we opened up for misunderstandings. In short, the DoF we display matches Rodgers' section 2.4.1. We tried to indicate this by defining the DoF as "measurements' degrees of freedom". Our comments seem to be based on the assumption that our DoF is the one described in Rodgers' 2.4.2. As this is not correct we don't go into details here.

We will describe the way we calculate DoF and clarify that it matches Rodgers 2.4.1.

line 13: Which surface parameter are you talking about, emissivity or surface temperature?

Both, and other ones. We will rewrite to something like: the various variables affecting

surface emission and reflectivity

line 6: I may have missed it somewhere but what is H?

We will change to H-polarisation.

line 8 (Fig 9): The problem with using only average is that we have no idea of the dispersion around the mean. A scatter plot presented with a 2D colorscale histogram give much more information on the overall performance of the retrieval. The author should consider this king of plot instead of presenting only the average.

The figure is based on so many retrievals that it would impossible to discern individual cases in a scatter plot, and we don't see this an option.

line 9: What do you mean by "good accuracy"? Is it in comparison to other related retrieval from other sensor?

Yes, this a vague statement. Will be rephrased.

line 14: Are the 5th and 95th percentile also averaged values?

Median. This information is found in the figure text.

line 17: This precision number for Zm and Dm are average precision, specify it somewhere!

Will be done.

line 4: Reference on ISMAR?

ISMAR is introduced and referenced in Sec 1.

line 8-9: last sentence says that ...

This section will be removed, following a recommendation of referee 1.

line 12-15: The cloudsat and caliop based algorithm like DARDAR for example, which retrieve IWC profile from the combination of both measurements, often show a layer of

supercooled water above the ice layer in the polar area. Are you planing to integrate this kind of case in your database in the futur. Is microwave sensitive to this kind of situation?

This is an interesting question, but, unfortunately, is an aspect of ICI observations that has got very little attention. To our best knowledge, nobody has studied the sensitivity of ICI to supercooled water for polar conditions. Indications to supercooled water for mid-latitude conditions are found in a manuscript in review (Pfreundschuh et al., AMTD).

This means that supercooled water probably must be considered in the generation of future retrieval databases. With the AMTD manuscript at hand, we now feel that it is motivated to suggest this. However, we want to here clarify that the generation of a complete retrieval database will be the subject of future studies, and it is today not known who will produce that database.

Another form of supercooled water is the liquid drops brought to sub-zero temperatures in updraft regions. These drops can have considerably size, and when present should impact on both ICI and CloudSat observations. We now notice that we missed to comment on this, and we will add a general comment/discussion of super-cooled water.

Best regards,

Patrick and co-authors

References:

Pfreundschuh, S., Eriksson, P., Buehler, S. A., Brath, M., Duncan, D., Larsson, R., and Ekelund, R.: Synergistic radar and radiometer retrievals of ice hydrometeors, Atmos. Meas. Tech. Discuss., https://doi.org/10.5194/amt-2019-369, in review, 2019.

Interactive comment on Atmos. Meas. Tech. Discuss., doi:10.5194/amt-2019-312, 2019.

Towards an operational Ice Cloud Imager (ICI) retrieval product

Patrick Eriksson[1], Bengt Rydberg[2], Vinia Mattioli[3], Anke Thoss[4], Christophe Accadia[3], Ulf Klein[5], and Stefan A. Buehler[6]

[1]Department of Space, Earth and Environment, Chalmers University of Technology, Gothenburg, Sweden
[2]Möller Data Workflow Systems AB, Gothenburg, Sweden
[3]EUMETSAT, Darmstadt, Germany
[4]Swedish Meteorological and Hydrological Institute (SMHI), Norrköping, Sweden
[5]European Space Agency/ESTEC, Noordwijk, Netherlands
[6]Department of Earth Sciences, Universität Hamburg, Hamburg, Germany

Correspondence: Patrick Eriksson (patrick.eriksson@chalmers.se)

Abstract. The second generation of the EUMETSAT Polar System (EPS-SG) will include the Ice Cloud Imager (ICI), the first operational sensor covering sub-millimetre wavelengths. Three copies of ICI will be launched that together will give a measurement time series exceeding 20 years. Due to the novelty of ICI, preparing the data processing is especially important and challenging. This paper focuses on activities related to the operational product planned, but also presents basic technical characteristics of the instrument. A retrieval algorithm based on Bayesian Monte Carlo integration has been developed. The main retrieval quantities are ice water path (IWP), mean mass height (Z_m) and mean mass diameter (D_m). A novel part of the algorithm is to fully present the inversion as a description of the posterior probability distribution. This is ~~to prefer~~ preferred for ICI as its retrieval errors not always follow Gaussian statistics. A state-of-the-art retrieval database is used to test the algorithm and to give an updated estimate of the retrieval performance. The degrees of freedom in measured radiances, and consequently the retrieval precision, vary with cloud situation. According to present simulations, IWP, Z_m and D_m can be determined with 90% confidence at best inside 50%, 700 m and 50 µm, respectively. The retrieval requires that the data from the thirteen channels of ICI are remapped to a common footprint. First estimates of the errors introduced by this remapping are also presented.

1 Introduction

Satellite data are today an indispensable part of numerical weather prediction (NWP), see e.g. Bauer et al. (2015). The first observations from space directed towards weather prediction were made during the early 1960s by the TIROS (Television InfraRed Observation Satellite) program, using optical and infrared sensors (Bandeen et al., 1961). According to Staelin et al. (1976), the first satellite-based microwave observations of Earth's atmosphere were made by Cosmos 243 and 384, launched by the Soviet Union in 1968 and 1970, respectively. Atmospheric humidity and liquid cloud water were measured using channels

at 22.235 and 37 GHz. These first, brief measurements (two weeks and two days, respectively) were followed by NEMS (Nimbus E Microwave Spectrometer) that was functional 2.4 years after its launch 1972 with Nimbus-5. The channels of NEMS were placed at 22.235, 31.4, 53.65, 54.9 and 58.86 GHz. The additional channels around 55 GHz gave information on the atmospheric temperature profile (Waters et al., 1975). Another microwave sensor onboard Nimbus-5 was ESMR (Electrically Scanning Microwave Radiometer), that had a single channel at 19.35 GHz and showed that rainfall can be detected from space (Kidd and Barrett, 1990).

More regular microwave soundings started around 1979 with the MSU (Microwave Sounding Unit) and SSM/T (Special Sensor Microwave – Temperature) sensor series. Both these instruments had only channels between 50 and 60 GHz (see e.g. Grody, 1983; Liou et al., 1981). The SSM/I (Special Sensor Microwave – Imager), introduced in 1987 had humidity, cloud liquid water and precipitation as main atmospheric targets, with channels at 19.4, 22.2, 37.0 and 85.5 GHz (see e.g. Schluessel and Emery, 1990), and thus extended the coverage of the microwave region ~~upwards~~to higher frequencies. The next main step was taken during the 1990s with the SSM/T-2 (Special Sensor Microwave – Humidity) and AMSU-B (Advanced Microwave Sounding Unit – B) instruments that both included three channels around 183.3 GHz (see e.g. Spencer et al., 1989; Saunders et al., 1995). A main motivation for extending the coverage up to 183 GHz was to obtain vertical information on humidity, and not only column values. Today a relatively high number of microwave sensors are operational, mainly in sun-synchronous orbits but also in other orbits, such as SAPHIR (Sondeur Atmospherique du Profil d'Humidite Intertropicale par Radiometrie) and GMI (Global precipitation mission Microwave Imager). Across-track and conically scanning microwave radiometers are by tradition denoted as imagers or sounders, respectively. The origin to this classification is that conically scanning instruments have tended to be optimised for deriving surface properties, while vertical sounding of the atmosphere has mainly been implemented as across-track instruments.

In NWP the capability of providing information on temperature and humidity with no or small impact of clouds has traditionally been seen as the main justification for launching microwave ~~receivers~~sounders. It has been recognised that passive microwave data also contain valuable information on clouds and precipitation and these features have been used in various stand-alone retrievals (e.g. Spencer et al., 1989; Weng et al., 2003; Andersson et al., 2010), but this fraction of the data has been rejected inside NWP as assimilation systems have been incapable of ~~dealing with~~ using these observations. This situation has started to change, and there are already indications of a strong increase of the relative impact of microwave data inside NWP (Geer et al., 2017).

The present growing impact of microwave data is mainly due to improved assimilation software in combination with increased computing power, but also new versions of the instruments having a higher number of channels has been beneficial. But one limitation has remained for two decades, that operational microwave observations are so far limited to frequencies below 195 GHz. This situation will change in 2023 with the launch of ICI (Ice Cloud Imager), that will extend the coverage up to 670 GHz. ICI is one of the instruments planned for the next generation of Metop satellites, see further Sec. 2. The frequencies 195 and 670 GHz ~~corresponds~~ correspond to wavelengths of 1.5 and 0.45 mm, respectively, and ICI will thus open up the "sub-millimetre region" for NWP.

The main objective of ICI is to provide data on humidity and ice hydrometeors, particularly the bulk ice mass. The advantage of using sub-millimetre observations for deriving such information was first pointed out by Frank Evans and coworkers in a series of articles (Evans and Stephens, 1995a, b; Evans et al., 1998, 1999, 2002). The initial idea was to have a sub-millimetre instrument onboard CloudSat to complement its cloud radar, but this part was later descoped.

The idea of a sub-millimetre cloud ice sounder was picked up again in a mission called CIWSIR, that was proposed to the European Space Agency ESA as an "Earth Explorer" in 2002 and again in 2005 (Buehler et al., 2007). CIWSIR was not selected, but ESA funded preparatory studies, that lead to a consolidated mission proposal called CloudIce for Earth Explorer 8 in 2010 (Buehler et al., 2012). It featured channels near 183.31, 243.20, 325.15, 448.00, and 664.00 GHz. Shortly thereafter, a similar sensor was also proposed for the international space station (ISS-ICE), with a reduced set of channels.

While CloudIce was not selected for Earth Explorer 8, it was taken as blueprint for the ICI instrument part of EUMETSAT Polar System - Second Generation (EPS-SG). Its channel configuration, given explicitly in Table 1, is identical to CloudIce, except that the number of channels near 183 GHz was reduced from 6 to 3.

ICI will be the first operational sub-millimetre mission, but measurements of our atmosphere at such wavelengths already exist by other instruments, mainly by limb sounding instruments. The main objective of these instruments is to monitor gases in the strato- and mesosphere, but at their lowest tangent altitudes they perform observations that have similarities with ICI. Retrievals of ice cloud mass have also been developed for all three sub-millimetre limb sounders launched so far; Aura MLS (Wu et al., 2006), Odin/SMR (Eriksson et al., 2007) and SMILES (Millán et al., 2013; Eriksson et al., 2014). Observations at 887 GHz were recently demonstrated by a "cubesat" mission (IceCube, Wu (2017)). The observation approach behind ICI has also been used by some airborne instruments. The pioneering instruments were MIR (Millimeter-wave Imaging Radiometer) and CoSSIR (Compact Scanning Submillimeter Imaging Radiometer) (Wang et al., 2001; Evans et al., 2005). More lately, ISMAR (International SubMillimetre Airborne Radiometer) has been developed largely to support the preparations for ICI (Fox et al., 2017). These instruments and the associated data analysis, besides their intrinsic scientific value, provided justification for ICI in the selection process and provide useful input when designing processing algorithms for ICI.

It is expected that ICI data will be used in two main ways. In NWP the data will mainly be ingested as basic radiances; for a review of challenges, expected benefits and approaches of "all-sky" assimilation, see Geer et al. (2018). The data of ICI can also be "inverted" in stand-alone algorithms to produce a number of geophysical quantities, see Buehler et al. (2012). The produced retrieval datasets can be of concern for short-term weather forecasting, but will likely mainly be used for different climate applications, such as the verification of global models made by the similar ice cloud products derived from limb sounders (e.g. Li et al., 2005; Eriksson et al., 2010; Jiang et al., 2012). This article describes activities performed under the auspices of EUMETSAT in preparation of a "day-one" retrieval product (i.e. the product released directly after commissioning), as well as to provide general support for using ICI data.

The ICI instrument and its main characteristics are introduced in Sec. 2, while the following Sec 3 outlines the retrieval algorithm in focus. The expected performance is investigated in Sec. 4 using simulated data. The two final sections provide an outlook and conclusions.

2 The Ice Cloud Imager

2.1 Overview of EPS-SG

The ICI mission is part of the EUMETSAT Polar System second generation system (EPS-SG). The space segment will consist of a two-satellite architecture, referred to as Metop-SG satellite A and B. There will be three satellite pairs, where each satellite will have a nominal lifetime of 7.5 years to span a total operational lifetime over 21 years. These satellites will fly, like present Metop, in a sun-synchronous mid-morning orbit at 09:30 local time of descending node. The altitude profile over the Earth geoid varies between 848 and 823 km (832 km mean altitude). The orbit repeat cycle will be 29 days (412 orbits per repeat cycle). The main ground-station will be Svalbard, but also McMurdo will be used to improve the timeliness of data. The ground segment ~~includes also~~ also includes regional ground stations for receiving Direct Data Broadcast. See further www.eumetsat.int/website/home/Satellites/FutureSatellites/EUMETSATPolarSystemSecondGeneration/index.html.

ICI will be onboard of the B satellites, also carrying MWI (Micro-Wave Imager), SCA (Scatterometer), RO (Radio Occultation sounder) and ~~A-CDS~~ ARGOS-4 (Advanced Data Collection System). In particular, MWI is a conically scanning radiometer which observes 18 frequencies ranging from 18 to 183 GHz. All channels up to 89 GHz will observe in dual polarisation, while only vertical polarisation will be provided for higher frequencies. MWI has the same requirements for incidence angle and fore-view observation as ICI. Combined, the MWI and ICI radiometers will provide an unprecedented set of microwave passive measurements, from 18.7 GHz up to 664 GHz.

It is noteworthy that MWI will cover the 118.75 GHz oxygen and the 183.15 GHz water vapour molecular transitions with four and five channels, respectively. This gives MWI sounding capabilities and this instrument narrows down the traditional separation between "imagers" and "sounders".

2.2 The receiver package

The ICI radiometer (Bergadá et al., 2016) consists of seven double sideband front-ends, operating with local oscillator (LO) frequencies of 183.31, 243,20, 325.15, 448.00 and 664.00 GHz. The frequencies 183.31, 325.15 and 448.00 correspond to three water vapour transitions, while 243,20 and 664.00 GHz are "window" channels (see Buehler et al., 2007, Fig. 10). There is a receiver at each of these LO frequencies providing data matching vertical (V) polarisation inside the atmosphere. At both the two window frequencies there is also a second receiver covering horizontal (H) polarisation. A spectrometer of filter-bank type is attached to each front-end. The receiver package will be kept in thermal balance by passive cooling. Presently, the receiver noise temperature is expected to be about 600, 900, 1700, 1500 and 2600 K at the five LO frequencies, respectively. See e.g. Janssen (1993) for an introduction to the concept of receiver noise temperature.

For the window frequency receivers the filter-bank consists of a single channel, while the other filter-banks have three channels each. Position and width of all the channels are reported in Table 1 and are visualised in Fig. 1.

Table 1. Specifications of the ICI receiver. ICI has double sideband receivers, indicated by ± in the third column, and the bandwidth refers to the width of single passbands, i.e. the intermediate frequency bandwidth. "NEΔT" and "Max bias" are reported as the requirements, and final performance should be better. Further comments are found in the text (the two last columns are discussed in Sec.3).

Channel		Frequencies	Bandwidth	Polari-	NEΔT	Max bias	Elevation	Azimuth	$\tau = 1$	Ozone
Name	ID	[GHz]	[GHz]	sation	[K]	[K]	offset [°]	offset [°]	[km]	[K]
ICI-1V	1	183.31±7.00	2.00	V	0.8	1.0	-0.780	0.000	0.8-3.8	0.1
ICI-2V	2	183.31±3.40	1.50	V	0.8	1.0	-0.780	0.000	2.8-5.6	0.1
ICI-3V	3	183.31±2.00	1.50	V	0.8	1.0	-0.780	0.000	3.8-6.8	0.1
ICI-4V	4	243.20±2.50	3.00	V	0.7	1.5	0.711	-3.398	0.0-2.5	0.1
ICI-4H	5	243.20±2.50	3.00	H	0.7	1.5	0.731	3.385	0.0-2.5	0.1
ICI-5V	6	325.15±9.50	3.00	V	1.2	1.5	-0.822	-2.226	1.6-4.4	0.2
ICI-6V	7	325.15±3.50	2.40	V	1.3	1.5	-0.822	-2.226	3.1-5.9	0.2
ICI-7V	8	325.15±1.50	1.60	V	1.5	1.5	-0.822	-2.226	4.4-7.4	0.9
ICI-8V	9	448.00±7.20	3.00	V	1.4	1.5	-0.822	2.240	4.5-7.2	0.1
ICI-9V	10	448.00±3.00	2.00	V	1.6	1.5	-0.822	2.240	6.0-8.9	0.1
ICI-10V	11	448.00±1.40	1.20	V	2.0	1.5	-0.822	2.240	7.2-10.2	0.3
ICI-11V	12	664.00±4.20	5.00	V	1.6	1.5	0.752	-1.367	4.5-7.1	1.6
ICI-11H	13	664.00±4.20	5.00	H	1.6	1.5	0.875	0.941	4.5-7.1	1.6

2.3 Antenna system, scanning and calibration

The receiver package is integrated with a conically scanning antenna system. The diameter of the main reflector is 0.26 m (slightly elliptical), and the system is rotating at 1.333 Hz (i.e. 45 r.p.m.). Atmospheric observations are made over about 120°, around the platform's (forward) flight direction. This gives a swath width of roughly 1500 km. The platform will perform yaw manoeuvres to keep the swath centred around the sub-nadir orbit track. During the remaining part of each rotation, calibration data will be obtained by observing "cold sky" and an internal calibration target that will have a temperature of around 300 K. The overall requirement on random (NEΔT) and systematic (bias) uncertainties of calibrated antenna temperatures are found in Table 1.

The horn antennas are designed to keep the angular resolution the same between channels (about 0.5°), but the footprints of the receivers still differ, as the antenna of each front-end is placed at a different position in the focal plane. The angular offsets are found in Table 1. The reference angle for the elevation offsets is 44.767°, measured from the nadir direction. This gives a configuration of instantaneous footprints at surface level as depicted in Fig 2, with surface incidence angles varying between 51.5° and 53.8°. The instantaneous footprint sizes at surface level are about 17/20 km along-track and 7.3/8.5 km across-track for the footprints having a positive/negative elevation offset (at -3 dB, and slightly varying with latitude). The angular movement inside the integration time increases the effective across-track size.

Although the combination of conical scanning and the platform's movement in total gives a continuous coverage over the swath, there will not be any perfect matches in horizontal coverage between the channels. Accordingly, some post-processing is required to obtain data suitable for an inversion using channels from more than one front-end. To support footprint "remapping" a high across-track sampling will be applied, data will be recorded every 0.661 ms. This corresponds to an across-track movement of the boresights between samples of about 2.7 km, giving ~~784~~ 785 samples/scan. The distance along-track between subsequent scans will be about 9 km. This gives substantial overlap of sample footprints, both in along- and across-track dimension, giving some freedom in setting the target resolution in the remapping of footprints. The requirement on final footprint size is 16 km (as average between along- and across-track resolution), and the requirement of e.g. NEΔT is defined for this horizontal resolution. The noise in individual samples will be higher. It is expected that averaging over four subsequent across-track samples will meet the requirements, and about 200 footprints/scan will effectively be provided. L1b data will only contain the original samples, the optimal remapping will differ depending on application.

3 Algorithm

3.1 Aim and constraints

The planned output of the EPS-SG Overall Ground Segment at EUMETSAT Headquarters includes the MWI-ICI-L2 product, that will contain retrievals based on MWI and ICI and be delivered in near real time. The objective of the IWP product of MWI-ICI-L2 is to provide a day-one, robust, retrieval that reflects the main information content of ICI radiances. For some centrally generated level 2 products, the EUMETSAT Satellite Application Facilities (SAFs) provide support by specifying the level 2 processing algorithms and share responsibility for the products. The SAF supporting Nowcasting (NWC-SAF) retains the scientific ownership of the IWP product and delivered the IWP algorithm theoretical basis definition (Rydberg, 2018). To allow for the procurement and implementation in the ground segment, the IWP algorithm definition had to be finished during 2018, with further changes in the algorithm specifications not to impact the basic architecture and design. The efforts so far have focused on the core algorithm and the retrieval database discussed below has been produced as an initial working basis. Future studies will be required to elaborate the final database. Additional products from ICI will be generated directly by the SAFs located at weather services in EUMETSAT member and co-operating states.

3.2 Overview

A first, crucial decision was the selection of retrieval approach. "Optimal estimation" (a.k.a. 1DVAR) was not selected as it would demand a forward model handling multiple scattering of polarised radiation and capable of providing the Jacobian with respect to the retrieval quantities. Such a model was simply not at hand. With respect to sub-millimetre cloud observations, optimal estimation has so far only been used for theoretically inclined studies (Birman et al., 2017; Grützun et al., 2018; Aires et al., 2019).

Further, the retrieval problem at hand is both non-linear and involves non-Gaussian statistics, and a more general solution of the Bayes theorem should be preferable. For practical reasons this leads to approaches based on a retrieval database (Rydberg et al., 2009). The most straightforward implementation can be denoted as BMCI (Bayesian Monte Carlo Integration), and has been the method of choice for Evans and coworkers (e.g. Evans et al., 2002).

There are close connections between BMCI and the standard use of neural nets (Pfreundschuh et al., 2018). Such neural nets (NN), a form of machine learning, have been applied on both simulated ICI data (Jimenez et al., 2007; Wang et al., 2017) and ISMAR field data (Brath et al., 2018). Both approaches (BMCI and NN) were considered initially, but NN was eventually rejected as it was found that a very high number of nets would be required and there was no established way to estimate retrieval uncertainties.

Following the selection of BMCI, a complete retrieval algorithm was designed (Fig. 3). The algorithm consists of two main parts, a series of pre-processing steps and the actual inversion by BMCI. Only the most critical aspects are discussed in the following sections, for details we refer to Rydberg (2018). The generation of the final retrieval database is a task of the future, but a possible manner to generate the database is still outlined in Sec 4.2.

3.3 Input and output

The main input to the retrieval algorithm are geo-located and calibrated antenna temperatures, i.e. L1b data. Data from a number of footprints will be involved in each inversion, being remapped to the target footprint specified (Sec. 3.4.1). The target footprint also governs the extraction of geophysical variables (Sec. 3.4.3). All important retrieval parameters are set by a configuration data structure.

The main output variables (L2) are ice water path (IWP), mean mass height (Z_m) and mean mass diameter (D_m). All these three variables are reported as percentiles of the estimated a posterior distribution (Sec. 3.5.1) and are defined as antenna weighted means. For example, the reported IWP is an estimation of

$$\mathrm{IWP} = \frac{\int_{z_0}^{\infty} \int_{\Omega} r(\Omega) \mathrm{IWC}(x(\Omega), y(\Omega), z) \, \mathrm{d}\Omega \, \mathrm{d}z}{\int_{\Omega} r(\Omega) \, \mathrm{d}\Omega}, \tag{1}$$

where r is the antenna ~~pattern~~(or radiation) pattern (in sr^{-1}, with the satellite as reference point), Ω is antenna pattern solid angle, x, y and z are Cartesian coordinates (with arbitrary origin) and IWC is ice water content:

$$\mathrm{IWC} = \int_0^{\infty} n(d_{\mathrm{veq}}) m(d_{\mathrm{veq}}) \, \mathrm{d}d_{\mathrm{veq}}, \tag{2}$$

where n is particle size distribution, m is particle mass and d_{veq} is equivalent volume diameter (ρ is the density of ice):

$$d_{\mathrm{veq}} = \sqrt[3]{6m/\pi\rho}. \tag{3}$$

That is, d_{veq} is the diameter of an "ice sphere" having the same mass. The start of the altitude integration in Eq. 1, z_0, is presently set to be the surface altitude, but it can be changed.

Mean mass height is defined as

$$Z_m = \frac{\int_{z_0}^{\infty} z \int_{\Omega} r(\Omega)\mathrm{IWC}(x(\Omega), y(\Omega), z)\,\mathrm{d}\Omega\,\mathrm{d}z}{\mathrm{IWP}}, \tag{4}$$

and mean mass size as (cf. e.g. Delanoë et al., 2014, Eq. 3)

$$D_m = \frac{\int_0^{\infty} d_{\mathrm{veq}}^4 \int_{z_0}^{\infty} \int_{\Omega} r(\Omega) n(d_{\mathrm{veq}})\,\mathrm{d}\Omega\,\mathrm{d}z\,\mathrm{d}d_{\mathrm{veq}}}{\int_0^{\infty} d_{\mathrm{veq}}^3 \int_{z_0}^{\infty} \int_{\Omega} r(\Omega) n(d_{\mathrm{veq}})\,\mathrm{d}\Omega\,\mathrm{d}z\,\mathrm{d}d_{\mathrm{veq}}}. \tag{5}$$

These equations are applied to calculate the IWP etc. of the database cases, and thus will represent the "true" values. As these equations take inhomogenities into account, both vertically and horizontally, the impact of "beamfilling" (Davis et al., 2007) will automatically be included in the estimated retrieval uncertainty.

The L2 data will contain further data, such as retrieved water vapour column, but the exact L2 format is not finalised and only the three main retrieval quantities are discussed below.

3.4 Pre-processing part

3.4.1 Target footprint and remapping of data

The exact geo-location of samples differs between channels (Sec 2.3), but the time integration of individual samples is shorter than the time period necessary to sweep out a single projected field of view. This allows for a footprint matching procedure by remapping of the original data. A toolbox for performing such remappings has been developed in a dedicated study issued by EUMETSAT (Rydberg and Eriksson, 2019). The toolbox is based on the Backus-Gilbert methodology (Backus and Gilbert, 1970; Stogryn, 1978), that earlier has successfully been applied for footprint-matching between various satellite data (e.g. Bennartz, 2000; Maeda and Imaoka, 2016).

In short, the Backus-Gilbert methodology can be used to obtain a set of optimal weighting coefficients for neighbouring samples, both within the scan and from adjacent scans, to create a remapped representation of the data matching a specified target footprint. A remapped value is a linear weighted combination of data of the channel of concern. The weights are found, after a trade-off analysis, by minimisation of a penalty function that considers both the effective noise of the remapped data and the fit to the target footprint.

The centre position of a retrieval is set by selecting one of the sample footprints of ICI-1V. The exact shape of the target footprint around this position will be determined later, but it is expected to be $\approx$16 km ~~semi-circular~~and close to circular. The effective noise of remapped samples should be equal or below the "NEΔT" reported in Table 1. Example results are found below, in Sec. 4.1.

3.4.2 Bias correction

The algorithm allows for a simple "bias correction" of the data:

$$T_{a,j}^c = a_j + b_j T_{a,j} \tag{6}$$

where $T^c_{a,j}$ is corrected antenna temperature for channel j, $T_{a,j}$ is the value as given by the remapping toolbox and a_j and b_j are channel specific coefficients.

The purpose of the bias correction is to remove systematic differences between remapped L1b data and the simulations behind the retrieval database. A bias can originate from e.g. calibration issues, the remapping and incorrect spectroscopic data in the simulations. This module will only be applied as a rough temporary solution if any bias is detected, until the source to the bias has been understood and corrected.

3.4.3 Geophysical data and RTTOV

The retrieval performance can be improved by incorporating various geophysical data. These data will be taken from the ECMWF forecast system. Data of dynamic character that will be used include: temperature, ozone and surface wind speed, while static data are various parameters to characterise surface altitude and type. The water vapour profile is also imported from ECMWF, but it is modified below the tropopause to have a constant relative humidity (a configuration setting). The logic behind this approach is to incorporate information on e.g. atmospheric temperatures and ozone from ECMWF (ICI has no temperature channels), while letting humidity be constrained by the ICI data. The last column in Table 1 gives the mean impact of ozone based on a set of simulations. The maximum impact found was 2.1 K, for ICI-11 and a mid-latitude winter scenario.

Using the ECMWF data as input, radiative transfer calculations will be performed applying the RTTOV software (Saunders et al., 2018), to obtain a first estimate of the atmospheric optical thickness and a reference antenna temperature (T^r_a). These calculations assume "clear-sky" conditions (i.e. no impact of hydrometeors), are run for all ICI channels and are discussed further below.

3.4.4 Channel selection

Modelling of surface effects will, at least initially, be a main obstacle for these retrievals. Simulating these effects for land surfaces is a challenge already at low microwave frequencies. The situation for water bodies is better, particularly as the TESSEM sea-surface emissivity parameterisation has been updated to cover the full frequency range of ICI (Prigent et al., 2017). Some validation of TESSEM has been made (using ISMAR), but presently relatively large model uncertainties are expected even for water surfaces.

The impact of surface effects on measured radiances depends mainly on the atmospheric transmission. The transmission varies strongly between the ICI channels, as exemplified in Fig. 4. It varies also with the atmospheric situation. Estimates of at what altitude the transmission to ICI equals e^{-1}, for clear-sky conditions, are found in the column "$\tau = 1$" of Table 1. The lowest altitudes are associated with driest atmospheric scenario considered, and vice versa. The table shows that surface effects is in general of no concern for e.g. ICI 7V, 10V, 11V and 11H, while for some channels the surface must always be considered.

As a consequence, an adaptive selection of data is required. A channel mask is formed by evaluating

$$\tau_{\mathrm{cs},j} + c_{\mathrm{hm}}\tau_{\mathrm{hm},j} \geq \tau^s_t \tag{7}$$

where $\tau_{\mathrm{cs},j}$ is the clear-sky optical thickness of channel j obtained by RTTOV, c_{hm} a configuration setting, $\tau_{\mathrm{hm},j}$ is estimated additional optical thickness due to hydrometeors and τ_t^s is a threshold value for surface type s. Data from channels fulfilling this criterion are included in the calculations. In the pre-processing part τ_{hm} is set to zero. The channel mask is re-evaluated as part of the BMCI module, then also including attenuation due to hydrometeors. Both c_{hm} and τ_t^s are configurable variables, where the later is specified for five different surface types. The selection of τ_t^s should consider to what extent surface emissivity variability is represented in the final retrieval database, as well as to what extent the error model in Sec. 3.5.3 covers remaining modelling uncertainty.

3.4.5 Detection of clear-sky data

The algorithm includes an optional module for identifying observations that with a high probability match clear-sky conditions, that thus can be set to give $\mathrm{IWP} = 0$ without doing an actual inversion. This procedure results in that the L2 structure can not be fully filled, e.g. the water vapour column will not be retrieved, and this module will only be activated if it will be necessary to decrease the overall calculation burden of the processing. As the module likely will not be applied, ~~no detailsare here given~~we refer to Rydberg (2018) for details.

3.5 Inversion part

3.5.1 Theory and retrieval representation

The retrieval is performed by the BMCI method (Sec. 3.2). For a description of BMCI and its relationship to Bayesian estimation, see e.g. Kummerow et al. (1996) or Pfreundschuh et al. (2018). In short, BMCI is based on a "retrieval database" consisting of n pairs of atmospheric state, x_i, and corresponding observation, $\boldsymbol{y}_i$, with the constraint that x_i is approximately distributed according to reality, i.e. represents the prior distribution of x. The essence of BMCI is, for a given measurement $\boldsymbol{y}$, to attribute a posterior probability, ~~$p(x_i|\boldsymbol{y})$~~$p_i(x_i|\boldsymbol{y})$, to each database state as

$$p_i(x_i|\boldsymbol{y}) = w_i a_i / \sum_{i=1}^{n} w_i a_i, \tag{8}$$

where w_i is a measure on the agreement between $\boldsymbol{y}$ and $\boldsymbol{y}_i$,

$$w_i = \exp(-\left[(\boldsymbol{y}-\boldsymbol{y}_i)^T \boldsymbol{S}_o^{-1}(\boldsymbol{y}-\boldsymbol{y}_i)\right]/2), \tag{9}$$

with $\boldsymbol{S}_o$ being the covariance matrix describing ~~observation uncertainties~~ measurement and forward model uncertainties (Kummerow et al., 1996). The factors a_i can be seen as a priori weights. They ~~are not standard, but are introduced to allow tailoring of the retrieval database to the specifics of the retrievals of concern~~can be used to optimise the retrievals for a given database size. For example, it could be justified to accept cases with $\mathrm{IWP} = 0$ only with some probability $r < 1$ during database generation (Sec. 5). If this thinning is performed, remaining database cases having $\mathrm{IWP} = 0$ will obtain $a_i = 1/r$ (instead of 1).

As Eq. 9 involves $\boldsymbol{S}_o$, this has the consequence that all uncertainties covered by this covariance matrix must approximately follow Gaussian statistics (as for 1DVAR). On the other hand, BMCI allows any a priori distribution of variables (unlike 1DVAR), and e.g. "outliers" can be included in the generation of the retrieval database.

The actual solution of BMCI is the estimated posterior distribution (as for all Bayesian methods), but it is unpractical to report sets of p. Some more compact description is needed. If the posterior distribution follows a Gaussian distribution it suffices to report the expectation value and the width of the distribution. ICI retrievals do not fall into this category and it was decided to instead use a more general description based on the cumulative distribution function, in the continuous case defined as

$$F_{x|\boldsymbol{y}}(x) = \int_{-\infty}^{x} p(x'|\boldsymbol{y})\mathrm{d}x', \tag{10}$$

where p denotes a probability density function, and in the framework of BMCI is obtained by summing ~~p_n for~~ the probability of all cases having $x_i < x$:

$$F_{x_i|\boldsymbol{y}}(x) = \sum_{x_i<x} p_i(x_i|\boldsymbol{y}). \tag{11}$$

Using Eq. 11, $F_{x|\boldsymbol{y}}$ is calculated on a wide grid of x-values. These data are then used to obtain the inverse distribution function, F^{-1}, numerically by interpolation to a set of fixed percentiles. A more descriptive name of F^{-1} is the quantile function. For example, $F^{-1}(0.5)$ is the median and the 90th percentile is $F^{-1}(0.9)$. Figure 5 exemplifies prior and posterior quantile functions.

It is presently planned to report the 5th, 16th, 50th, 84th and 95th percentiles in the L2 data. If the retrieval must be condensed to a single value, the first candidate to "best estimate" should be the 50th percentile. The other percentiles can be used in different ways. For example, if the 5th percentile for IWP is > 0 then a correct detection of ice hydrometeors is highly probable. The 16th/84th percentile range matches $\pm 1\sigma$ for a Gaussian distribution. The true value is between the 5th and 95th percentiles with a probability of 90%, etc.

3.5.2 ~~Measurement vector and uncertainties~~

~~The measurement vector ($\boldsymbol{y}$) incorporates data from channels fulfilling the optical thickness criterion of Eq. 7 as a difference:~~

$$\Delta T_{a,j} = T^c_{a,j} - T^r_{a,j}$$

~~where $T^c_{a,j}$ is defined by Eq. 6 and $T^r_{a,j}$ is a simulated antenna temperature (by RTTOV, Sec. 3.4.3). To match this, the retrieval database contains both a full (all-sky) simulation and one (clear-sky) matching $T^r_{a,j}$.~~

~~The matrix $\boldsymbol{S}_o$ (Eq. 9) shall represent both instrument and simulation uncertainties. It is kept diagonal in lack of relevant information on uncertainty correlations between channels, but also for calculation efficiency reasons. The variances σ^2 are set as~~

$$\sigma^2_j = \mathrm{NE}\Delta\mathrm{T}^2_j + (\Delta\epsilon T_{\mathrm{skin}} e^{-\tau_{e,j}})^2 + (c\Delta T_{a,j})^2,$$

where NEΔT is uncertainty due to thermal noise and calibration. The second term aims at representing impact of unknown surface emissivity, where $\Delta\epsilon$ is emissivity uncertainty, $T_{\rm skin}$ is the ECMWF surface skin temperature and it is assumed that the emissivity is relatively high (impact through reflection of down-welling radiation neglected). The last term covers uncertainty in modelling of hydrometeor scattering, where it is assumed that the modelling error is proportional to the deviation from the clear-sky reference simulation. NEΔT for each channel (j), $\Delta\epsilon$ for water and land, and c are constants, part of the configuration data.

3.5.2 Database extraction and iterations

Not all database cases are included in the BMCI summation, a filtering is done based on surface type, pressure, wind speed and temperature, as well as ΔT_a (as defined below in Eq. 12). Wind speed is effectively only considered applicable only over water. The database extraction is done in an iterative manner, where the filter limits are adjusted with an iteration counter, in order to fetch both the most relevant and a sufficient number of matches. The filtering does not involve latitude or season. This results in that e.g. a tropical database case can influence the inversion of a mid-latitude summer measurement, if there is a match in surface temperature etc.

An additional iteration scheme has been added around the core BMCI calculations. A first reason is to better make use of the observations in situations with significant hydrometeor contents. The optical thickness associated with hydrometeors is estimated alongside of the L2 data in each iteration. Based on this updated estimate of the total optical thickness, Eq. 7 is reevaluated for all channels. If this results in that more channels can be included, BMCI is reiterated with the new channel mask. This iteration is important as the channels sensitive to the surface in a clear-sky situation, and thus ignored in the initial iteration, are the most important ones to obtain good estimates at high IWP.

The second reason is to handle the fact that the retrieval database only provides a discrete coverage of the distribution of $\boldsymbol{y}$. If one $\boldsymbol{y}_i$ happens to agree closely with $\boldsymbol{y}$, one w_i can be orders of magnitude bigger than all other w and the summation in Eq. 8 will be dominated by one database case. While the median value found can be realistic, this results in an underestimation of the retrieval uncertainty. It could also be the case that no $\boldsymbol{y}_i$ gives a significant match with $\boldsymbol{y}$. Both these situations are primarily handled by increasing the variances in $\boldsymbol{S}_o$, effectively making the "search radius" larger. If this does not suffice, channels will be rejected until an acceptable number of significant weights are obtained.

For further details of the filtering and iteration schemes, see Rydberg (2018). All critical parameters are part of the configuration data.

3.5.3 Measurement vector and uncertainties

The measurement vector ($\boldsymbol{y}$) incorporates data from channels fulfilling the optical thickness criterion of Eq. 7 as a difference:

$$\Delta T_{a,j} = T^c_{a,j} - T^r_{a,j} \tag{12}$$

where $T^c_{a,j}$ is defined by Eq. 6 and $T^r_{a,j}$ is a simulated antenna temperature (by RTTOV, Sec. 3.4.3). To match this, the retrieval database contains the difference between a full (all-sky) simulation and one (clear-sky) matching $T^r_{a,j}$.

The matrix $\boldsymbol{S}_o$ (Eq. 9) represents both instrument and simulation uncertainties. It is kept diagonal in lack of relevant information on uncertainty correlations between channels. The knowledge regarding such correlations is especially poor for surface emissivity. The variances σ^2 are set as

$$\sigma_j^2 = \mathrm{NE}\Delta\mathrm{T}_j^2 + (\Delta\epsilon T_{\mathrm{skin}} e^{-\tau_{\mathrm{cs},j}})^2 + (c\Delta T_{a,j})^2, \quad (13)$$

where $\mathrm{NE}\Delta\mathrm{T}$ is uncertainty due to thermal noise and calibration. The second term aims at representing the impact of unknown surface emissivity, where $\Delta\epsilon$ is emissivity uncertainty, T_{skin} is the ECMWF surface skin temperature, and it is assumed that the emissivity is relatively high. The antenna temperature is then approximately $T_a = \epsilon T_{\mathrm{skin}} e^{-\tau_{\mathrm{cs},j}} + T_e(1 - e^{-\tau_{\mathrm{cs},j}})$, where T_e is an effective temperature of the atmosphere, and thus $\mathrm{d}T_a/\mathrm{d}\epsilon \approx T_{\mathrm{skin}} e^{-\tau_{\mathrm{cs},j}}$.

The last term covers uncertainty in modelling of hydrometeor scattering. To our best knowledge, no investigation of such modelling errors has been made. The uncertainty is zero for clear-sky conditions, and it should in general increase with the strength of scattering. Based on these two simple observations, we decided to simply model the error as proportional to the deviation from the clear-sky reference simulation. $\mathrm{NE}\Delta\mathrm{T}$ for each channel (j), $\Delta\epsilon$ for water and land, and c are constants, part of the configuration data.

4 Performance tests

4.1 Remapping of data

Samples from all ICI channels will be convolved into the field of view of ICI-1V. This section summarises the main findings obtained by applying the Backus-Gilbert toolbox developed (Sec. 3.4.1)~~on detailed radiative transfer simulations~~.

4.1.1 Simulate test data

To test the toolbox four full orbits were simulated. The orbit parameters were taken from Metop-A (orbits 4655, 4656, 6985 and 9744). Geophysical data for the time of the four orbits were taken from ERA5 (mate.copernicus.eu/climate-reanalysis). ERA5 lacks data on precipitation of convective nature. To compensate for this, precipitation was added from a separate database (provided by Alan Geer at ECMWF), based on similarities of large-scale precipitation profiles and some other variables. Using these data, radiances were simulated for all MWI and ICI channels, covering an area broader than the instrument's swath and representing a set of incidence angles.

These simulations were done by running the ARTS software in its three-dimensional mode (Eriksson et al., 2011). Absorption due to gases and liquid water content was calculated following Rosenkranz (1993, 1998) and Ellison (2007), and surface emissivities following Prigent et al. (2017) and Aires et al. (2011). The size distribution of rain drops and ice hydrometeors were set following Abel and Boutle (2012) and Field et al. (2007), respectively. Particle properties were taken from Eriksson et al. (2018), applying ID25 for rain and IDs 15 and 20 for ice hydrometeors (the name of these habits are found Table 2 below).

Using the set of pre-calculated pencil-beam radiances as a "look-up"-table, antenna weighted brightness temperatures could be generated with a relatively low calculation burden taking full account of MWI's and ICI's scanning and footprints

characteristics, for different assumptions of the exact syncing between the instruments. In all parts, the WGS-84 reference ellipsoid was applied.

4.1.2 Main findings

The assumption here is that the goal of the remapping is to obtain data as would be observed with a synthetic instrument having a common footprint for all channels (implying the same surface incidence angle for all channels). As will be shown, this can not be achieved perfectly. However, these "errors" can at least partly be considered in the retrieval process and the final impact can be relatively low. Most importantly, the basic impact of different incidence angles can be included in both 1DVAR and BMCI retrievals.

A bias-free convolution ~~has been~~ was demonstrated as long as the remapping does not involve a change in incidence angle. However, this is strictly true only for ICI-2V and ICI-3V. These two channels share bore-sight with ICI-1V, but the antenna patterns differ somewhat and a remapping is still required.

Figure 6 exemplifies the issues that appear for the other channels, having an incidence angle that differs from the one of ICI-1V (Table 1). Considerable remapping errors are found for ICI-11V. The elevation offset of this channel deviates to ICI-1V with 1.53°, that scales to a ∼2 degree lower incidence angle at surface level. This angular difference results in a remapping error even in the absence of hydrometeors, as exemplified by the upper-left portion of the simulated area. The remapping generates data that are 0.4 - 0.6 K too warm, as the toolbox can not compensate for the original difference in incidence angle. The "clear-sky" brightness temperature is higher at a lower incidence angle.

The same effect can be noted for areas with relative homogeneous cloud distributions, but brightness temperatures vary more strongly with incidence angle in cloudy conditions and the error for ICI-11V is here instead about $0.5 - 2$ K (see e.g. the area directly south of 0°N 10°E). Further, at the edges of areas with hydrometeors even higher errors can be noted, as well as errors of opposite sign. These errors originate in horizontal inhomogenities. The target footprint is defined at the altitude of the reference ellipsoid ~~. This means that line-of-sights of observations and the corresponding ones after remapping cross at the ellipsoid but deviate at altitudes~~ and the remapping is optimal for this altitude. However, the effective footprint for some altitude inside the atmosphere ~~. The horizontal distance between the two line-of-sights~~ is the one at zero altitude projected upwards following the incidence angle of each channel. That is, the footprints will not overlap perfectly, with a horizontal displacement that increases with altitude~~, being~~ . As example, for ICI-11V it is about 700 m at 12 km~~for ICI-11V.~~ . Hence, the noted errors match the change in brightness temperature for horizontal shifts of that order. However, the atmospheric data used in the simulations do not have this high horizontal resolution and the magnitude of these errors are just indicative.

The errors found for ICI-5V (Fig. 6) show a similar spatial pattern, but have the reversed sign and are of lower magnitude. This is expected as the zenith offset of ICI-5V is only 0.04°smaller than the one of ICI-1V, in contrast to the larger, positive shift for ICI-11V.

4.2 Generation of retrieval database

Retrieval databases for ICI must so far be generated by radiative transfer simulations. The input to the simulations can be obtained from atmospheric models providing a ~~sufficient~~ sufficiently detailed description of hydrometeors (Wang et al., 2017; Brath et al., 2018). This approach relies on that the model mimics reality with sufficient accuracy, as it represents the a priori for the BMCI retrieval. Another option is to base the simulations directly on observations as far as possible. As the spatial resolution of ICI is limited, the most important input is information on vertical and horizontal structures in hydrometeor fields. Today such data are available through cloud radars, even on global scale by ~~the CloudSat one~~ CloudSat (Stephens et al., 2002).

The cloud radar data can be used in various ways. Some options are explored by Evans et al. (2002, 2012), while the results reported below are based on the methodology developed in Rydberg et al. (2007, 2009). The basic idea is to produce simulated passive observations that are consistent with the basic information provided by the radar, i.e. measured reflectivities. This is done for some assumption on particle size and shape distributions. That is, external retrievals of e.g. IWC are not involved, the mapping from radar reflectivities to particle optical properties at the frequencies of the passive data is done by an internal, implicit retrieval. The retrieval database should contain simulations for a set of different particle assumptions, to reflect the variability and our limited knowledge of particle shapes and sizes. Remaining atmospheric data can be taken from some analysis (such as ECMWF's ERA5), but this still represents a drawback of the approach as consistency is not guaranteed. Most importantly, corrections are likely required to avoid improbable relative humdities where hydrometeors are present.

4.3 ICI retrieval performance

4.3.1 Test retrieval database

At this stage, the simulations are based on stretches of CloudSat ~~data~~reflectivites, selected randomly and with no preference regarding longitudes, land/ocean etc.. That is, the simulations have two dimensions, vertical and along-track. The ICI slant geometry and antenna pattern are represented fully inside this 2-d geometry. So far the extension of the antenna pattern in the across-track dimension is neglected, but can be included by mapping the CloudSat data to three dimensions (Rydberg et al., 2009). Consideration of the antenna pattern is required to avoid systematic modelling biases due to "beamfilling" (Davis et al., 2007).

The procedure applied to map radar reflectivities to microwave radiances is described in detail by Ekelund et al. (2019). The radiative transfer calculations were performed with the ARTS software (Buehler et al., 2018), using its interface to the RT4 (Evans and Stephens, 1995b) scattering solver. RT4 is applied following the "independent beam approximation" (see further Sec. 5), inside the two-dimensional atmosphere formed based on the CloudSat data. Absorption due to gases and liquid water was treated as in Sec. 4.1.

The microphyscial models applied are described in Table 2. For mid and high latitudes also simulations with a modified gamma distribution (for two habits) were produced, but the resulting D_m was found to be ~~unrealisticly high~~ unrealistically high (a significant fraction even above 2 mm) and this part of the database is here rejected. Oriented and melting particles are so far ignored.

Table 2. Combinations of particle size distribution and habit model included in the test retrieval database. McFarquhar and Heymsfield (1997) is shortened to MH97. Field et al. (2007) defined a tropical and a mid-latitude version of their size distribution, and both are used. Each habit model consists of single scattering data selected from Eriksson et al. (2018), ~~specified as the data's id-number inside that database. For example, 15+20 stands for a mix between thick plates (id 15)~~ where both name and ~~large plate aggregates (id 20)~~id-number are specified.

Hydro-meteor	Size distribution	Habit ~~model~~ name	ID	Latitude region
Ice	Field et al. (2007)	Sector snowflake	3	Tropics
Ice	Field et al. (2007)	Evans snow aggregate	1	Tropics
Ice	MH97	Thick plate+Large plate aggregate	15+20	~~tropics~~Tropics
Ice	Field et al. (2007)	Evans snow aggregate	1	Mid and high
Rain	Abel and Boutle (2012)	Liquid sphere	25	Global

Observations over both water and land were simulated. Ocean surface emissivity was modelled according to Prigent et al. (2017)~~, while~~ . In lack of any model for ICI's frequency range, land emissivity was simply set to vary randomly around ~~0.8 in lack of a proper model~~0.9 (with a log-normal distribution). The data used below contain in total $6.2 \cdot 10^6$ cases~~.~~, based on 1373 CloudSat orbits between Sep 2015 and Jan 2016.

Besides the retrieval database, ~~some data were~~ a smaller dataset was also simulated for channels 16 - 21 of ATMS (Weng et al., 2012) and a statistical comparison to actual observations was made. The simulated data were generated exactly as done for the retrieval database, except that the footprint averaging followed the specifications of ATMS. Example results are displayed in Fig 7. The peak in the distribution around 255 K corresponds to "clear-sky" situations (low level cloud can still be present), while most cases below ~230 K should contain influences of ice hydrometeors. The agreement between simulations and observations is high down to about 200 K. For lower brightness temperatures the simulations show higher occurrence rates than the observations. This deviation is at least partly a consequence of that the full antenna pattern and particle orientation are not yet considered in the simulations. The better agreement for nadir simulations, where ATMS has a smaller footprint, indicates the impact of the first of these two effects. By assuming totally random particle orientation radar back-scattering is under-estimated and our procedure will generate clouds with a high bias in IWC. There is a compensating effect when simulating the passive data, by a similar under-estimation of extinction, but it is smaller, at least for angles away from nadir where particle orientation has a smaller impact on the projected cross-section (Brath et al., 2019).

The approach behind the database generation reproduces GMI (Draper et al., 2015) data in a similar manner, even when focusing on the tropical Pacific where deep convective systems control the impact of ice hydrometeors on ICI and the radiative transfer simulations are especially challenging ~~(Ekelund et al., submitted manuscript)~~(Ekelund et al., 2019).

A similar comparison is found in Fig. 13 of Geer and Baordo (2014). They obtained a poorer agreement with observations, with an underestimation starting at about 225 K. Similar particle models were used and the better agreement found here is likely a consequence of that the simulations are based on CloudSat, and not model data. The agreement is similar for the

other ATMS channels considered, see Rydberg (2018). A graphical manner for exploring if the retrieval database covers the multi-dimensional space spanned by the observations to be inverted is found in Brath et al. (2018, Fig. 2).

4.3.2 Degrees of freedom

As an introduction to the information provided by ICI, Fig. 8 displays an estimate of the measurements' degrees of freedom (~~DOF) . The DOF~~ DoF) for tropical conditions. The DoF can be seen as a measure on the effective number of channels.

Each DoF-value is calculated by finding the (left) eigenvectors ($\boldsymbol{E}$) of the simulated set of measurement vectors in consideration (without noise added). These eigenvectors and the covariance matrix ($\boldsymbol{S_y}$) of the data are related as:

$$\boldsymbol{S_y} = \boldsymbol{E}\boldsymbol{\Lambda}\boldsymbol{E}^T \tag{14}$$

where Λ is a diagonal matrix, holding the eigenvalues. See e.g. Eriksson et al. (2002) for further details. The uncertainty due to thermal noise, in the eigenvalue space, is

$$\boldsymbol{S_\Lambda} = \boldsymbol{E}\boldsymbol{S_\epsilon}\boldsymbol{E}^T, \tag{15}$$

where $\boldsymbol{S_\epsilon}$ has $\mathrm{NE}\Delta\mathrm{T}^2$ as its diagonal elements and is zero elsewhere (cf. Eq. 13). As $\boldsymbol{S_\epsilon}$ is diagonal, also $\boldsymbol{S_\Lambda}$ will be diagonal due to properties of the eigenvectors (orthonormality). The number of diagonal elements in $\boldsymbol{S_y}$ that are larger than the corresponding value in $\boldsymbol{S_\Lambda}$ can be taken as the DoF. This calculation of DoF is essentially the same as the analysis described in Sec. 2.4.1 of Rodgers (2000), but is somewhat more general as it is based on $\boldsymbol{S_y}$ and does not involve the Jacobian matrix, so it can be easily computed even in cases where Jacobians are not available.

For very low IWP and most wet atmospheres, the ~~DOF~~ DoF is only two. For these conditions, ICI is primarily sensitive to humidity in the middle and upper troposphere. The ~~DOF~~ DoF increases with decreasing IWV, as humidity at lower altitudes then gets a growing impact. The ~~DOF~~ DoF is here about three, consistent with the fact that ICI has three channels around each water vapour transition covered (1V-3V, 5V-7V and 9V-11V, respectively), and that there is a high redundancy in information between these groups of channels (which together give an improved precision for water vapour retrievals). Figure 4 shows that the two innermost 448 GHz channels cover higher altitudes than the other channels, but it appears that these two channels add little information in single-footprint retrievals due to a relatively high noise (Table 1). A further analysis of ICI's overall performance for clear-sky conditions is left for a future study. For most dry atmospheres, there is also a surface contribution to the ~~DOF from the surface~~DoF, mainly by channels 4V and 4H, from the various variables affecting surface emission and reflectivity.

The ~~DOF~~ DoF is considerably higher at high IWP. The maximum ~~DOF~~ DoF in Fig. 8 is eight, but the true number is likely higher. The figure is based on simulations only including totally random particle orientation and thus the full information given by the dual polarisation channels is not reflected. The simulations lack also melting particles and still use a relatively low number of particle models, and the full variability of hydrometeors is probably not yet reflected.

There is an intermediate range, extending between about 10 and 500 $\mathrm{g/m^2}$, where ~~DOF~~ DoF is increasing with IWP. This analysis shows that ICI acts mainly as a coarse humidity sounder for IWP below $\sim$10 $\mathrm{g/m^2}$, but, as designed, provides more

rich data with increasing ice hydrometeor content. This indicates that ICI is suitable for measuring IWP, but the ~~DOF~~ DoF gives no information on retrieval precision or if other quantities also can be constrained.

4.3.3 Overall performance

The retrieval performance was estimated by repeatedly dividing the data generated between a retrieval database and test data (Fig. 9). The algorithm described in Sec. 3 was followed, except that no footprint remapping or run of RTTOV was performed. Since particle orientation is not yet included, these retrievals did not include the extra 243 and 664 GHz channels that measure ~~H~~H-polarisation. Noise was added following the NEΔT of Table 1, but present tests indicate that lower noise will actually be achieved. Both these aspects should lead to a conservative estimate of the performance at low IWP, or ~~compensating~~ compensate for error sources not yet considered. The results in Fig. 9 are averages of retrievals over both water and land.

The best performance is found for tropical conditions where IWP above about 50 $\mathrm{g/m^2}$ can be retrieved ~~with good accuracy~~without a clear bias. ICI provides information also for lower IWP, down to about 10 $\mathrm{g/m^2}$, but then with an increasing influence of a priori information causing a low bias. This bias occurs because the a priori is dominated by cases having IWP=0. Accordingly, the bias could be decreased strongly by an independent method of cloud detection, effectively removing all, or most, IWP=0 from the a priori distribution.

The retrieval precision in Fig. 9 is reported as the range between the 5th and 95th percentile. This range corresponds to a 50% uncertainty above about 200 $\mathrm{g/m^2}$. The precision is poorer for lower IWP, particularly on the 5th percentile side. This percentile reaches IWP = 0 when the true value is $\sim$ 15 $\mathrm{g/m^2}$. Mean altitude, Z_m is well estimated over its full range (for the type of ice clouds of concern for ICI), i.e. between about 4 and 12 km, with a median precision in the order of 700 m. The retrieval of D_m is best between 175 and 400 µm, where the median precision is about 50 µm, but the retrievals should be competitive between about 100 and 800 µm.

~~Results~~ As a contrast, results for mid-latitude late autumn/winter conditions are also found in Fig. 9. There are likely ~~highly~~ higher uncertainties in these simulations (e.g., they involve only a single particle habit) and these results should be approached with more care. Compared to tropical conditions, the performance is poorer, especially for IWP below 100 $\mathrm{g/m^2}$. This is the case because the ice hydrometeors here are found at lower altitudes, often below the sounding range of the high frequency channels. Low IWP is best estimated by the 664 GHz channels, but they have sensitivity only down to about 5 km (Fig. 4). Low altitude clouds also make the choice of τ_t^s (Eq. 7) critical. For these test retrievals, it was set to 1 for oceans and 3 for all other surface types. Z_m is retrieved without any significant bias between 2 and 10 km, but the posterior distribution is highly skewed below 3 km. That is, the 50th percentile is in general a good estimate, but the retrieval can not fully rule out considerably higher Z_m. The accuracy is good for D_m between 150 and 600 µm, while there is a quickly growing ~~high~~ low bias above 650 µm.

These results do not deviate significantly from earlier similar studies. The most similar one is Jimenez et al. (2007), particularly as it also used IWP, Z_m, and D_m as retrieval quantities. They found a better retrieval performance for low IWP, ~~that is likely a consequence of that smaller retrieval databases were used and less error sourceswere considered~~which likely is due to a smaller retrieval database and fewer considered error sources. Our results should be more realistic, albeit ~~possibly made in a~~

~~conservativemanner~~ somewhat conservative, as explained at the start of this section. Wang et al. (2017) made a study focusing on relatively severe weather over Europe and obtained similar IWP accuracy as reported here. They did not consider Z_m and D_m, but retrieval of separate hydrometeor classes as well as joint inversion of data from MWI and ICI. When comparing results between studies, the error range definition considered must be ~~noticed~~noted. We use a ~~more broad~~ wider range (matching $\pm 2\sigma$) compared to most others.

4.3.4 ~~Test inversions~~

~~As a general sanity check, the algorithm has been been tested practically on data from some ISMAR flights. Some modifications were needed to handle the ISMAR observations. The main additional obstacles are that the flight altitude and observation angle vary, and the retrieval database must contain simulations for all combinations of altitude and angle considered. A quantitative assessment of these retrievals was not possible due to lack of any independent estimates of IWP, but we judged the results as reasonable. At least no obvious flaws were found. These various results have been presented at conferences (e.g. Eriksson et al., 2016) and the details are not repeated here.~~

5 Outlook

The basic algorithm will not be modified until some time after the launch of ICI and the main concern for the coming years is to refine the retrieval database generation. A required extension is to include particle orientation~~. The~~, as shown by Defer et al. (2014) and Gong and Wu (2017). The first data on scattering properties at sub-millimetre wavelengths of oriented particles have just been presented (Brath et al., 2019). Varying orientation distributions should be used in the database generation. Scattering solvers handling oriented particles include RT4 (Evans and Stephens, 1995b) and DOIT (Emde et al., 2004).

In the database used in this work, a strict separation between liquid and ice hydrometers was assumed. This is a simplification in several ways. Super-cooled liquid cloud droplets are common in the atmosphere (e.g. Zhang et al., 2010), frequently as part of "mixed-phase" clouds. Results in Pfreundschuh et al. (2019) indicate that ICI has some sensitivity to such super-cooled liquid water and it should thus be considered in future work. Also the super-cooled liquid water in updraft regions of convective cells should be taken into account, especially as the drops here can be of mm-size and the liquid water content can reach several $\mathrm{g/m^3}$ (Lawson et al., 2015). This should lead to a significant impact on both CloudSat and ICI data. Finally, the impact of melting ~~particles~~ ice hydrometeors should be assessed and ~~be~~ included if found relevant. However, data on single scattering properties ~~are lacking for both these considerations~~of such particles are still lacking for the frequency range of ICI.

A broader range of particle size distributions and particle shapes should be used, compared to the simulations used in this work. The simulations should of course make use of most recent studies ~~on particle size distributions and particle shapes~~of these particle properties, preferably applying data tailored for each cloud type of concern. ISMAR should be an essential tool for validating microphysical assumptions. A first study of this type has already been performed (Fox et al., 2019).

~~A~~ On the instrument side, a more detailed treatment of the full antenna pattern is needed. This will increase the calculation burden, but to what extent is not yet known. The present assumption is that an independent beam approximation (IBA) can be

applied, i.e. that the radiance at one location can be sufficiently well estimated by a simulation of one-dimensional character. ~~However, test~~ Test simulations have revealed that this is not true for all situations, but full three-dimensional, polarised simulations can so far only be performed by computationally costly Monte Carlo methods~~. For this reason~~ , therefore IBA would be to prefer. The error by applying IBA is being assessed as part of a EUMETSAT fellowship project.

As discussed in Sec. 4.1, the necessary spatial remapping of channels causes some errors due to the differences in incidence angle. These remapping errors must either be incorporated in the generation of the database or be treated as an observation uncertainty. In the later case, an error model must be derived to set $\boldsymbol{S}_o$ (Eq. 9) accordingly. The information on temperature and ozone obtained from ECMWF (Sec. 3.4.3) has uncertainty and the resulting impact on the retrievals has not yet been studied. The same is true for errors in assumed spectroscopic parameters, used to calculate the absorption due to gases. As ICI will operate in a relatively unexplored wavelength region, considerably spectroscopic uncertainties can not be ruled out at this point (Mattioli et al., 2019). Also here ISMAR should be ~~an~~ a useful tool for validation.

A number of retrieval configuration settings need to be determined. For example, the optical thickness thresholds (τ_t^s, Eq. 7) should be reevaluated at some point, then preferably with improved knowledge, obtained by ISMAR, of the variability of surface emissivity at the frequencies of ICI. Another example is that a clear strategy for the database thinning discussed in Sec. 3.5.1 is lacking, only rudimentary tests have so far been made.

In a longer perspective, joint inversions of data from MWI and ICI shall be considered. Such synergistic retrievals should be especially beneficial for obtaining consistent data on liquid and ice hydrometeor properties (Wang et al., 2017). The remapping toolbox is prepared to handle this extension, but application of BMCI becomes more problematic as dealing with the combined measurements drastically increases the required retrieval database size. Machine learning could be an alternative. In Pfreundschuh et al. (2018) it is shown that quantiles of the posterior distribution can be estimated by neural networks more efficiently than with BMCI.

6 Conclusions

Ice hydrometeors presently constitute one of the components in Earth's atmosphere that are least constrained by ~~present~~ observation and modelling systems. There is even a persistent large spread among zonal means of IWP (Waliser et al., 2009; Eliasson et al., 2011; Duncan and Eriksson, 2018). ICI will provide observations that could be used to decrease these uncertainties both inside weather forecasting and stand-alone retrievals, as well as by model verification through "satellite simulators". ICI does not offer the spatial resolution of cloud radars, such as the CloudSat one, but has the swath width needed for obtaining semi-global coverage on a daily basis.

The focus of this article is the ICI retrieval algorithm (Rydberg, 2018) that will be applied operationally at EUMETSAT. At the time of the algorithm selection, BMCI was judged a safer option than existing machine learning alternatives. However, since machine learning is developing rapidly, future scientific retrieval algorithms may well employ it.

The "day-one" algorithm described here aims at extracting the basic information of ICI on ice hydrometeors, which is the ice water path, as well as cloud altitude and particle size. ICI has the potential to also provide profiles of ice water content

(Wang et al., 2017; Birman et al., 2017; Grützun et al., 2018; Aires et al., 2019), but that possibility is so far left for research groups to investigate.

An innovative aspect of the new algorithm is that, to our best knowledge, it is the first example where the retrieval result is presented fully as a description of the posterior distribution (by reporting five percentiles), and not as the expectation value and some uncertainty value. This more general approach is to prefer for ICI as the retrieval uncertainty can exhibit a highly skewed distribution.

The core algorithm has successfully been tested using ISMAR and simulated ICI data, but the final retrieval performance is mainly determined by the quality of the retrieval database provided to the processing system. Such a database has been produced for test purposes and to provide updated estimates of the retrieval precision. The database reflects the state of the art, but the retrieval error estimates should still be considered as tentative because some tools needed to cover the full complexity of the observations are still lacking.

It is hard to find stringent uncertainty estimates of other IWP retrievals, but we note that the global mean of IWP given by the DARDAR inversions (mainly based on CloudSat) changed by 26% between the two most recent versions (Cazenave et al., 2019). Based on present simulations, ICI will deliver a similar accuracy at least above IWP = $200\,\mathrm{g/m^2}$. Above this IWP, there is no intrinsic cause of bias in the retrievals, and the precision for single retrievals is $\pm 50\%$ (at quantiles matching $\pm 2\sigma$).

The use of ICI in numerical weather prediction (NWP) is not discussed here, but several activities described are also relevant for this application. The most notable example should be the development of ice hydrometeor single scattering data (Eriksson et al., 2018), that is of direct relevance for "all-sky" assimilation of ICI radiances. A problem common for NWP and stand-alone retrievals is how to incorporate the effect of ice particle orientation without making the radiative transfer calculations too costly. This extension is required to make full use of ICI's double polarisation channels at 243 and 664 GHz.

In this paper we have tried to reflect the efforts already performed to prepare for inversions using ICI, but also to indicate the work that remains to be done. Combining the data of ICI and MWI is an especially interesting prospect for future extensions. That combination can possibly provide a relatively full view of water in all its three phases (gas, liquid and ice).

As a last remark we would like to stress that ICI will provide the first "operational" observations of our atmosphere in the sub-millimetre region and its data will cover more than 20 years. This will give the weather forecasting and climate communities a new important data source.

Author contributions. PE and BR participated in most of the activities described and lead the manuscript writing. VM and CA contributed to the work, supervising and reviewing the algorithm development in its various phases and contributed to the manuscript writing. AT is in charge of the algorithm development inside NWC-SAF and has revised the manuscript. UK is main ICI scientist at ESA/ESTEC and has provided the technical description. SB has contributed input and text, and revised the manuscript.

Code availability. The footprint remapping toolbox can be obtained by contacting EUMETSAT. It will be distributed "as is" with no warranties and on the condition of no redistribution, as well as that this article and the EUMETSAT study with Contract EUM/C0/18/4600002075/CJA are cited where used. Other numerical results in the article are based on various Matlab and Python scripts, kept in local SVN repositories, that can be obtained by contacting the first two authors. Usage of these scripts requires assess to the ARTS and Atmlab packages, available at www.radiativetransfer.org.

Competing interests. The authors declare that they have no conflict of interest.

Acknowledgements. A first version of the algorithm, based on neural nets, was outlined by Gerrit Holl as project scientist at SMHI. The development of footprint remapping routines for ICI was performed under the EUMETSAT study " Application of optimal interpolation procedures to EPS-SG MWI and ICI ", Contract EUM/C0/18/4600002075/CJA. Figure 8 was produced by Simon Pfreundschuh (Chalmers). The science advisory group around MWI and ICI has given feedback on the work described here. This project would not have been possible without the many individuals that are contributing to the technical development of ICI and the development of the ARTS infrastructure. The preparations for ICI performed at Chalmers University of Technology are largely funded by grants from the Swedish National Space Agency (SNSA). The contribution of SB was supported by the Deutsche Forschungsgemeinschaft (DFG, German Research Foundation) under Germany's Excellence Strategy — EXC 2037 'Climate, Climatic Change, and Society' — Project Number: 390683824.

References

Abel, S. and Boutle, I.: An improved representation of the raindrop size distribution for single-moment microphysics schemes, Q. J. R. Meteorol. Soc., 138, 2151–2162, 2012.

Aires, F., Prigent, C., Bernardo, F., Jiménez, C., Saunders, R., and Brunel, P.: A Tool to Estimate Land-Surface Emissivities at Microwave frequencies (TELSEM) for use in numerical weather prediction, Q. J. R. Meteorol. Soc., 137, 690–699, 2011.

Aires, F., Prigent, C., Buehler, S. A., Eriksson, P., Milz, M., and Crewell, S.: Towards more realistic hypotheses for the information content analysis of cloudy/precipitating situations – Application to an hyper-spectral instrument in the microwaves, Q. J. R. Meteorol. Soc., pp. 1–14, https://doi.org/10.1002/qj.3315, 2019.

Andersson, A., Fennig, K., Klepp, C., Bakan, S., Graßl, H., and Schulz, J.: The Hamburg ocean atmosphere parameters and fluxes from satellite data–HOAPS-3, Earth Syst. Sci. Data, 2, 215–234, 2010.

Backus, G. and Gilbert, F.: Uniqueness in the inversion of inaccurate gross Earth data, Philos. Trans. R. Soc. London, Ser. A, 266, 123–192, 1970.

Bandeen, W. R., Hanel, R. A., Licht, J., Stampfl, R., and Stroud, W.: Infrared and reflected solar radiation measurements from the TIROS II meteorological satellite, J. Geophys. Res., 66, 3169–3185, 1961.

Bauer, P., Thorpe, A., and Brunet, G.: The quiet revolution of numerical weather prediction, Nature, 525, 47, 2015.

Bennartz, R.: Optimal convolution of AMSU-B to AMSU-A, J. Atmos. Ocean. Technol., 17, 1215–1225, https://doi.org/10.1175/1520-0426(2000)017<1215:OCOABT>2.0.CO;2, 2000.

Bergadá, M., Labriola, M., González, R., Palacios, M., Marote, D., Andrés, A., García, J., Sánchez-Pascuala, D., Ordóñez, L., Rodríguez, M., et al.: The Ice Cloud Imager (ICI) preliminary design and performance, in: 2016 14th Specialist Meeting on Microwave Radiometry and Remote Sensing of the Environment (MicroRad), pp. 27–31, IEEE, 2016.

Birman, C., Mahfouf, J.-F., Milz, M., Mendrok, J., Buehler, S. A., and Brath, M.: Information content on hydrometeors from millimeter and sub-millimeter wavelengths, Tellus A: Dyn. Meteo. and Ocean., 69, https://doi.org/10.1080/16000870.2016.1271562, 2017.

Brath, M., Fox, S., Eriksson, P., Harlow, R. C., Burgdorf, M., and Buehler, S. A.: Retrieval of an ice water path over the ocean from ISMAR and MARSS millimeter and submillimeter brightness temperatures, Atmos. Meas. Tech., 11, 611–632, https://doi.org/10.5194/amt-11-611-2018, 2018.

Brath, M., Ekelund, R., Eriksson, P., Lemke, O., and Buehler, S. A.: Microwave and submillimeter wave scattering of oriented ice particles, Atmos. Meas. Tech. Discuss, 2019, 1–38, https://doi.org/10.5194/amt-2019-382, https://www.atmos-meas-tech-discuss.net/amt-2019-382/, 2019.

Buehler, S. A., Jimenez, C., Evans, K. F., Eriksson, P., Rydberg, B., Heymsfield, A. J., Stubenrauch, C., Lohmann, U., Emde, C., John, V. O., Sreerekha, T. R., and Davis, C. P.: A concept for a satellite mission to measure cloud ice water path and ice particle size, Q. J. R. Meteorol. Soc., 133, 109–128, https://doi.org/10.1002/qj.143, 2007.

Buehler, S. A., Defer, E., Evans, F., Eliasson, S., Mendrok, J., Eriksson, P., Lee, C., Jiménez, C., Prigent, C., Crewell, S., Kasai, Y., Bennartz, R., and Gasiewski, A. J.: Observing ice clouds in the submillimeter spectral range: the CloudIce mission proposal for ESA's Earth Explorer 8, Atmos. Meas. Tech., 5, 1529–1549, https://doi.org/10.5194/amt-5-1529-2012, 2012.

Buehler, S. A., Mendrok, J., Eriksson, P., Perrin, A., Larsson, R., and Lemke, O.: ARTS, the Atmospheric Radiative Transfer Simulator – version 2.2, the planetary toolbox edition, Geosci. Model Dev., 11, 1537–1556, https://doi.org/10.5194/gmd-11-1537-2018, 2018.

Cazenave, Q., Ceccaldi, M., Delanoë, J., Pelon, J., Groß, S., and Heymsfield, A.: Evolution of DARDAR-CLOUD ice cloud retrievals: new parameters and impacts on the retrieved microphysical properties, Atmos. Meas. Tech., 12, 2819–2835, https://doi.org/10.5194/amt-12-2819-2019, 2019.

Davis, C., Evans, K., Buehler, S., Wu, D., and Pumphrey, H.: 3-D polarised simulations of space-borne passive mm/sub-mm midlatitude cirrus observations: a case study, Atmos. Chem. Phys., 7, 4149–4158, 2007.

Defer, E., Galligani, V. S., Prigent, C., and Jimenez, C.: First observations of polarized scattering over ice clouds at close-to-millimeter wavelengths (157 GHz) with MADRAS on board the Megha-Tropiques mission, J. Geophys. Res., 119, 12–301, 2014.

Delanoë, J., Heymsfield, A. J., Protat, A., Bansemer, A., and Hogan, R.: Normalized particle size distribution for remote sensing application, J. Geophys. Res., 119, 4204–4227, 2014.

Draper, D. W., Newell, D. A., Wentz, F. J., Krimchansky, S., and Skofronick-Jackson, G. M.: The global precipitation measurement (GPM) microwave imager (GMI): Instrument overview and early on-orbit performance, IEEE Journal of Selected Topics in Applied Earth Observations and Remote Sensing, 8, 3452–3462, 2015.

Duncan, D. I. and Eriksson, P.: An update on global atmospheric ice estimates from satellite observations and reanalyses, Atmos. Chem. Phys., 18, 11 205–11 219, https://doi.org/10.5194/acp-18-11205-2018, 2018.

Ekelund, R., Eriksson, P., and Pfreundschuh, S.: Using passive and active microwave observations to constrain ice particle models, Atmos. Meas. Tech. Discuss, 2019, 1–30, https://doi.org/10.5194/amt-2019-293, 2019.

Eliasson, S., Buehler, S. A., Milz, M., Eriksson, P., and John, V. O.: Assessing observed and modelled spatial distributions of ice water path using satellite data, Atmos. Chem. Phys., 11, 375–391, https://doi.org/10.5194/acp-11-375-2011, 2011.

Ellison, W.: Permittivity of pure water, at standard atmospheric pressure, over the frequency range 0–25 THz and the temperature range 0–100 C, Journal of physical and chemical reference data, 36, 1–18, 2007.

Emde, C., Buehler, S. A., Davis, C., Eriksson, P., Sreerekha, T. R., and Teichmann, C.: A polarized discrete ordinate scattering model for simulations of limb and nadir longwave measurements in 1D/3D spherical atmospheres, J. Geophys. Res., 109(D24), D24 207, https://doi.org/10.1029/2004JD005140, 2004.

Eriksson, P., Jiménez, C., Bühler, S., and Murtagh, D.: A Hotelling transformation approach for rapid inversion of atmospheric spectra, J. Quant. Spectrosc. Radiat. Transfer, 73, 529–543, https://doi.org/10.1016/S0022-4073(01)00175-3, 2002.

Eriksson, P., Ekström, M., Rydberg, B., and Murtagh, D. P.: First Odin sub-mm retrievals in the tropical upper troposphere: ice cloud properties, Atmos. Chem. Phys., 7, 471–483, www.atmos-chem-phys.net/7/471/2007/, 2007.

Eriksson, P., Rydberg, B., Johnston, M., Murtagh, D. P., Struthers, H., Ferrachat, S., and Lohmann, U.: Diurnal variations of humidity and ice water content in the tropical upper troposphere, Atmos. Chem. Phys., 10, 11 519–11 533, https://doi.org/10.5194/acp-10-11519-2010, 2010.

Eriksson, P., Buehler, S. A., Davis, C. P., Emde, C., and Lemke, O.: ARTS, the atmospheric radiative transfer simulator, Version 2, J. Quant. Spectrosc. Radiat. Transfer, 112, 1551–1558, https://doi.org/10.1016/j.jqsrt.2011.03.001, 2011.

Eriksson, P., Rydberg, B., Sagawa, H., Johnston, M. S., and Kasai, Y.: Overview and sample applications of SMILES and Odin-SMR retrievals of upper tropospheric humidity and cloud ice mass, Atmos. Chem. Phys., 14, 12 613–12 629, https://doi.org/10.5194/acp-14-12613-2014, 2014.

Eriksson, P., Ekelund, R., Mendrok, J., Rydberg, B., Buehler, S., Brath, M., Thoss, A., Fox, S., Accadia, C., and Mattioli, V.: Preparations for Metop SG Ice Cloud Imager retrievals, in: 8th IPWG and 5th IWSSM Joint Workshop, Bologna, Italy, www.isac.cnr.it/~ipwg/meetings/bologna-2016/Bologna2016_Orals/2-5_Eriksson.pdf, 2016.

Eriksson, P., Ekelund, R., Mendrok, J., Brath, M., Lemke, O., and Buehler, S. A.: A general database of hydrometeor single scattering properties at microwave and sub-millimetre wavelengths, Earth Syst. Sci. Data, 10, 1301–1326, https://doi.org/10.5194/essd-10-1301-2018, 2018.

Evans, K. F. and Stephens, G. L.: Microwave radiative transfer through clouds composed of realistically shaped ice crystals. Part I: Single scattering properties, J. Atmos. Sci., 52, 2041–2057, 1995a.

Evans, K. F. and Stephens, G. L.: Microwave radiative transfer through clouds composed of realistically shaped ice crystals. Part II: Remote sensing of ice clouds, J. Atmos. Sci., 52, 2058–2072, https://doi.org/10.1175/1520-0469(1995)052<2058:MRTTCC>2.0.CO;2, 1995b.

Evans, K. F., Walter, S. J., Heymsfield, A. J., and Deeter, M. N.: Modeling of submillimeter passive remote sensing of cirrus clouds, J. Appl. Meteorol., 37, 184–205, 1998.

Evans, K. F., Evans, A. H., Nolt, I. G., and Marshall, B. T.: The prospect for remote sensing of cirrus clouds with a submillimeter-wave spectrometer, J. Appl. Meteorol., 38, 514–525, 1999.

Evans, K. F., Walter, S. J., Heymsfield, A. J., and McFarquhar, G. M.: Submillimeter-Wave Cloud Ice Radiometer: Simulations of retrieval algorithm performance, J. Geophys. Res., 107, https://doi.org/10.1029/2001JD000709, 2002.

Evans, K. F., Wang, J. R., Racette, P. E., Heymsfield, G., and Li, L.: Ice cloud retrievals and analysis with the compact scanning submillimeter imaging radiometer and the cloud radar system during CRYSTAL FACE, J. Appl. Meteorol., 44, 839–859, 2005.

Evans, K. F., Wang, J. R., Starr, D. O., Heymsfield, G., Li, L., Tian, L., Lawson, R. P., Heymsfield, A. J., and Bansemer, A.: Ice hydrometeor profile retrieval algorithm for high-frequency microwave radiometers: application to the CoSSIR instrument during TC4, Atmos. Meas. Tech., 5, 2277–2306, https://doi.org/10.5194/amt-5-2277-2012, 2012.

Field, P. R., Heymsfield, A. J., and Bansemer, A.: Snow size distribution parameterization for midlatitude and tropical ice clouds, J. Atmos. Sci., 64, 4346–4365, 2007.

Fox, S., Lee, C., Moyna, B., Philipp, M., Rule, I., Rogers, S., King, R., Oldfield, M., Rea, S., Henry, M., et al.: ISMAR: an airborne submillimetre radiometer, Atmos. Meas. Tech., 10, 477–490, 2017.

Fox, S., Mendrok, J., Eriksson, P., Ekelund, R., O'Shea, S. J., Bower, K. N., Baran, A. J., Harlow, R. C., and Pickering, J. C.: Airborne validation of radiative transfer modelling of ice clouds at millimetre and sub-millimetre wavelengths, Atmos. Meas. Tech., 12, 1599–1617, https://doi.org/10.5194/amt-12-1599-2019, 2019.

Geer, A., Baordo, F., Bormann, N., Chambon, P., English, S., Kazumori, M., Lawrence, H., Lean, P., Lonitz, K., and Lupu, C.: The growing impact of satellite observations sensitive to humidity, cloud and precipitation, Q. J. R. Meteorol. Soc., 143, 3189–3206, 2017.

Geer, A. J. and Baordo, F.: Improved scattering radiative transfer for frozen hydrometeors at microwave frequencies, Atmos. Meas. Tech., 7, 1839–1860, https://doi.org/10.5194/amt-7-1839-2014, 2014.

Geer, A. J., Lonitz, K., Weston, P., Kazumori, M., Okamoto, K., Zhu, Y., Liu, E. H., Collard, A., Bell, W., Migliorini, S., et al.: All-sky satellite data assimilation at operational weather forecasting centres, Q. J. R. Meteorol. Soc., 144, 1191–1217, 2018.

Gong, J. and Wu, D. L.: Microphysical properties of frozen particles inferred from Global Precipitation Measurement (GPM) Microwave Imager (GMI) polarimetric measurements, Atmos. Chem. Phys., 17, 2741–2757, 2017.

Grody, N. C.: Severe storm observations using the microwave sounding unit, J. Climate Appl. Meteor., 22, 609–625, 1983.

Grützun, V., Buehler, S. A., Kluft, L., Mendrok, J., Brath, M., and Eriksson, P.: All-sky information content analysis for novel passive microwave instruments in the range from 23.8 to 874.4 GHz, Atmos. Meas. Tech., 11, 4217–4237, https://doi.org/10.5194/amt-11-4217-2018, 2018.

Janssen, M. A.: An introduction to the passive microwave remote sensing of atmospheres., Atmospheric remote sensing by microwave radiometry, pp. 1–35, 1993.

Jiang, J. H., Su, H., Zhai, C., Perun, V. S., Del Genio, A., Nazarenko, L. S., Donner, L. J., Horowitz, L., Seman, C., Cole, J., et al.: Evaluation of cloud and water vapor simulations in CMIP5 climate models using NASA "A-Train" satellite observations, J. Geophys. Res., 117, 2012.

Jimenez, C., Buehler, S. A., Rydberg, B., Eriksson, P., and Evans, K. F.: Performance simulations for a submillimetre wave cloud ice satellite instrument, Q. J. R. Meteorol. Soc., 133, 129–149, https://doi.org/10.1002/qj.134, 2007.

Kidd, C. and Barrett, E.: The use of passive microwave imagery in rainfall monitoring, Remote Sensing Reviews, 4, 415–450, 1990.

Kummerow, C., Olson, W. S., and Giglio, L.: A simplified scheme for obtaining precipitation and vertical hydrometeor profiles from passive microwave sensors, IEEE T. Geosci. Remote, 34, 1213–1232, 1996.

Lawson, R. P., Woods, S., and Morrison, H.: The microphysics of ice and precipitation development in tropical cumulus clouds, J. Atmos. Sci., 72, 2429–2445, 2015.

Li, J.-L., Waliser, D., Jiang, J., Wu, D., Read, W., Waters, J., Tompkins, A., Donner, L., Chern, J.-D., Tao, W.-K., et al.: Comparisons of EOS MLS cloud ice measurements with ECMWF analyses and GCM simulations: Initial results, Geophys. Res. Lett., 32, 2005.

Liou, K.-N., Aufderhaar, G. C., and Nipko, P. T.: Some examples of the effects of clouds and precipitation on the temperature profile retrieval for DMSP SSM/T microwave sounders, J. Appl. Meteorol., 20, 821–825, 1981.

Maeda, T. and Imaoka, Y. T. K.: GCOM-W1 AMSR2 level 1R product: Dataset of brightness temperature modified using the antenna pattern matching technique, IEEE T. Geosci. Remote, 54, 770–782, 2016.

Mattioli, V., Accadia, C., Prigent, C., Crewell, S., Geer, A., Eriksson, P., Fox, S., Pardo, J. R., Mlawer, E., Cadeddu, M., Bremer, M., Breuck, C. D., Smette, A., Cimini, D., Turner, E., Mech, M., Marzano, F. S., Brunel, P., Vidot, J., Bennartz, R., Wehr, T., Michele, S. D., and John, V.: Atmospheric gas absorption knowledge in the sub-millimeter: Modeling, field measurements, and uncertainty quantification, Bull. Amer. Meteorol. Soc., accepted, https://doi.org/10.1175/BAMS-D-19-0074.1, 2019.

McFarquhar, G. M. and Heymsfield, A. J.: Parameterization of tropical cirrus ice crystal size distributions and implications for radiative transfer: Results from CEPEX, J. Atmos. Sci., 54, 2187–2200, 1997.

Millán, L., Read, W., Kasai, Y., Lambert, A., Livesey, N., Mendrok, J., Sagawa, H., Sano, T., Shiotani, M., and Wu, D. L.: SMILES ice cloud products, J. Geophys. Res., 118, 6468–6477, https://doi.org/10.1002/jgrd.50322, 2013.

Pfreundschuh, S., Eriksson, P., Duncan, D., Rydberg, B., Håkansson, N., and Thoss, A.: A neural network approach to estimating a posteriori distributions of Bayesian retrieval problems, Atmos. Meas. Tech., 11, 4627–4643, https://doi.org/10.5194/amt-11-4627-2018, 2018.

Pfreundschuh, S., Eriksson, P., Buehler, S. A., Brath, M., Duncan, D., Larsson, R., and Ekelund, R.: Synergistic radar and radiometer retrievals of ice hydrometeors, Atmos. Meas. Tech. Discuss, 2019, 1–35, https://doi.org/10.5194/amt-2019-369, 2019.

Prigent, C., Aires, F., Wang, D., Fox, S., and Harlow, C.: Sea-surface emissivity parametrization from microwaves to millimetre waves, Q. J. R. Meteorol. Soc., 143, 596–605, 2017.

Rodgers, C. D.: Inverse methods for atmospheric sounding: theory and practice, vol. 2, World scientific, 2000.

Rosenkranz, P. W.: Absorption of microwaves by atmospheric gases, in: Atmospheric remote sensing by microwave radiometry, edited by Janssen, M. A., pp. 37–90, John Wiley & Sons, Inc., 1993.

Rosenkranz, P. W.: Water vapor microwave continuum absorption: A comparison of measurements and models, Radio Sci., 33, 919–928, (correction in 34, 1025, 1999), ftp://mesa.mit.edu/phil/lbl_rt, 1998.

Rydberg, B.: EPS-SG ICI ice water path product: ATBD. SAF/NWC/LEO-EPSSG/ATBD/IWP-ICI Issue 2.1, Rev. 2, Tech. rep., EUMETSAT NWCSAF, www.nwcsaf.org, -> Documentation -> Archive, Search: IWP-ICI, 2018.

Rydberg, B. and Eriksson, P.: Backus-Gilbert footprint matching methodology applied on MWI and ICI observations, Tech. rep., EUMETSAT, www.eumetsat.int/website/home/Data/ScienceActivities/ScienceStudies/index.html, contract EUM/CO/18/4600002075/CJA, 2019.

Rydberg, B., Eriksson, P., and Buehler, S. A.: Prediction of cloud ice signatures in sub-mm emission spectra by means of ground-based radar and in-situ microphysical data, Q. J. R. Meteorol. Soc., 133, 151–162, https://doi.org/10.1002/qj.151, 2007.

Rydberg, B., Eriksson, P., Buehler, S. A., and Murtagh, D. P.: Non-Gaussian Bayesian retrieval of tropical upper tropospheric cloud ice and water vapour from Odin-SMR measurements, Atmos. Meas. Tech., 2, 621–637, www.atmos-meas-tech.net/2/621/2009/, 2009.

Saunders, R., Hocking, J., Turner, E., Rayer, P., Rundle, D., Brunel, P., Vidot, J., Roquet, P., Matricardi, M., Geer, A., et al.: An update on the RTTOV fast radiative transfer model (currently at version 12), Geosci. Model Dev., 11, 2717–2737, 2018.

Saunders, R. W., Hewison, T. J., Stringer, S. J., and Atkinson, N. C.: The radiometric characterization of AMSU-B, IEEE Transactions on microwave theory and techniques, 43, 760–771, 1995.

Schluessel, P. and Emery, W. J.: Atmospheric water vapour over oceans from SSM/I measurements, Int. J. Remote Sens., 11, 753–766, 1990.

Spencer, R. W., Goodman, H. M., and Hood, R. E.: Precipitation retrieval over land and ocean with the SSM/I: Identification and characteristics of the scattering signal, J. Atmos. Ocean. Technol., 6, 254–273, 1989.

Staelin, D. H., Kunzi, K. F., Pettyjohn, R. L., Poon, R. K. L., Wilcox, R. W., and Waters, J. W.: Remote sensing of atmospheric water vapor and liquid water with the Nimbus 5 microwave spectrometer, J. Appl. Meteorol., 15, 1204–1214, 1976.

Stephens, G. L., Vane, D. G., Boain, R. J., Mace, G. G., Sassen, K., Wang, Z., Illingworth, A. J., O'connor, E. J., Rossow, W. B., Durden, S. L., et al.: The CloudSat mission and the A-Train: A new dimension of space-based observations of clouds and precipitation, Bull. Amer. Meteorol. Soc., 83, 1771–1790, 2002.

Stogryn, A.: Estimates of brightness temperatures from scanning radiometer data, IEEE Trans. Antennas Propag., AP-26, 720–726, 1978.

Waliser, D. E., Li, J.-L. F., Woods, C. P., Austin, R. T., Bacmeister, J., Chern, J., Genio, A. D., Jiang, J. H., Kuang, Z., Meng, H., Minnis, P., Platnick, S., Rossow, W. B., Stephens, G. L., Sun-Mack, S., Tao, W.-K., Tompkins, A. M., Vane, D. G., Walker, C., and Wu, D.: Cloud ice: A climate model challenge with signs and expectations of progress, J. Geophys. Res., 114, D00A21, https://doi.org/10.1029/2008JD010015, 2009.

Wang, D., Prigent, C., Aires, F., and Jimenez, C.: A statistical retrieval of cloud parameters for the millimeter wave Ice Cloud Imager on board MetOp-SG, IEEE Access, 5, 4057–4076, 2017.

Wang, J. R., Liu, G., Spinhirne, J. D., Racette, P., and Hart, W. D.: Observations and retrievals of cirrus cloud parameters using multichannel millimeter-wave radiometric measurements, J. Geophys. Res., 106, 15 251–15 263, 2001.

Waters, J. W., Kunzi, K. F., Pettyjohn, R. L., Poon, R. K. L., and Staelin, D. H.: Remote sensing of atmospheric temperature profiles with the Nimbus 5 microwave spectrometer, J. Atmos. Sci., 32, 1953–1969, 1975.

Weng, F., Zhao, L., Ferraro, R. R., Poe, G., Li, X., and Grody, N. C.: Advanced microwave sounding unit cloud and precipitation algorithms, Radio Sci., 38, 2003.

Weng, F., Zou, X., Wang, X., Yang, S., and Goldberg, M.: Introduction to Suomi national polar-orbiting partnership advanced technology microwave sounder for numerical weather prediction and tropical cyclone applications, J. Geophys. Res., 117, 2012.

Wu, D. L.: Upper-tropospheric cloud ice from IceCube, in: AGU Fall Meeting Abstracts, 2017.

Wu, D. L., Jiang, J. H., and Davis, C.: EOS MLS cloud ice measurements and cloudy-sky radiative transfer model, IEEE T. Geosci. Remote, 44, 1156–1165, 2006.

Zhang, D., Wang, Z., and Liu, D.: A global view of midlevel liquid-layer topped stratiform cloud distribution and phase partition from CALIPSO and CloudSat measurements, J. Geophys. Res., 115, 2010.

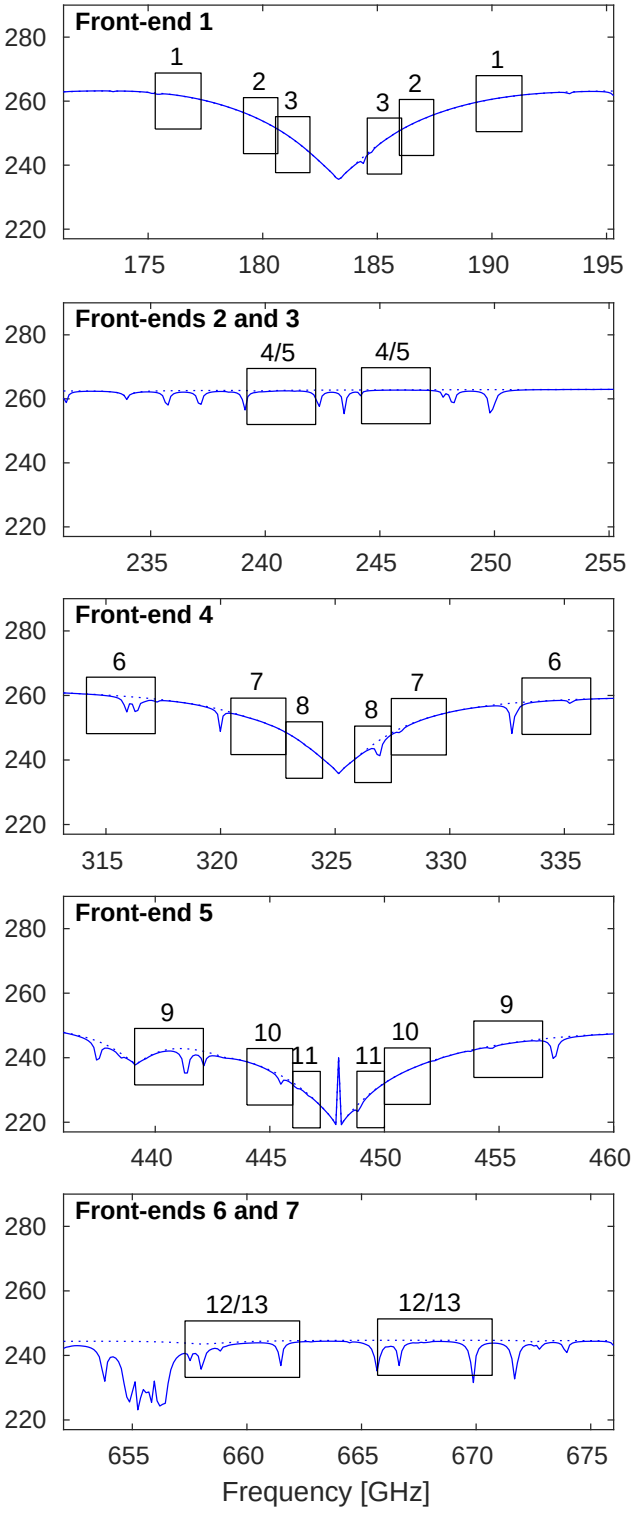

Figure 1. Frequency coverage of the sidebands for each ICI channel. The simulated spectrum (blue line) is based on a mid-latitude winter scenario. The dotted lines are simulations ignoring ozone.

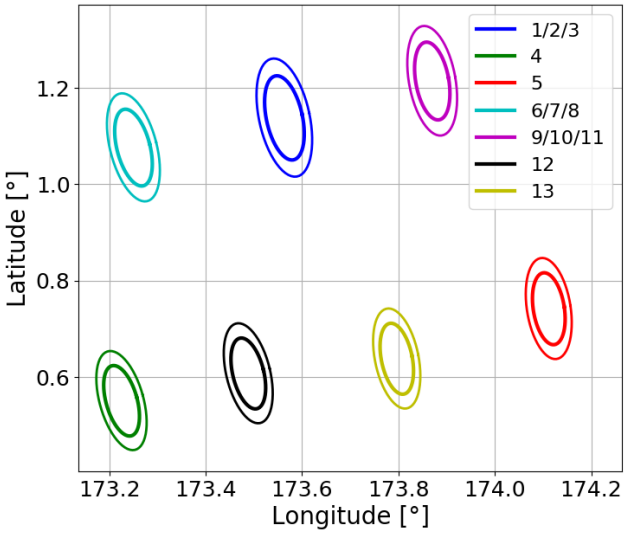

Figure 2. Instantaneous ICI footprints. The inner and outer contours represent the -3 and -6 dB level of normalised antenna patterns. The assumed sensor position is 6.9°S, 175.3°E at an altitude of 824.5 km.

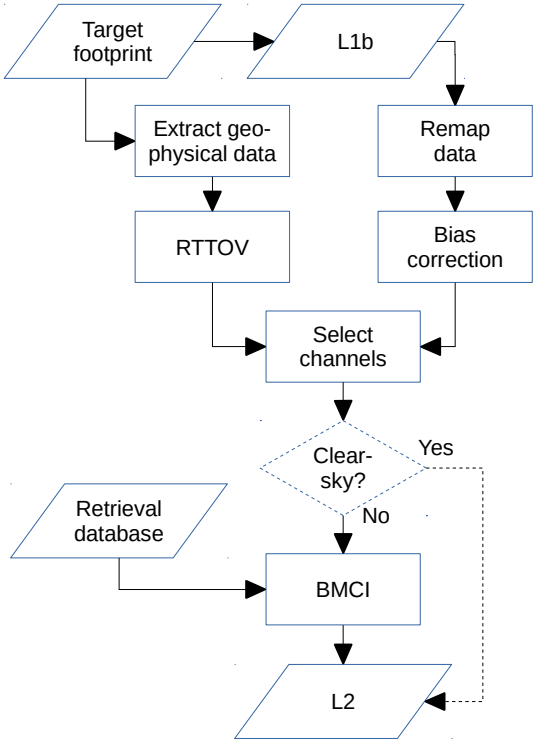

Figure 3. The overall data flow of the algorithm.

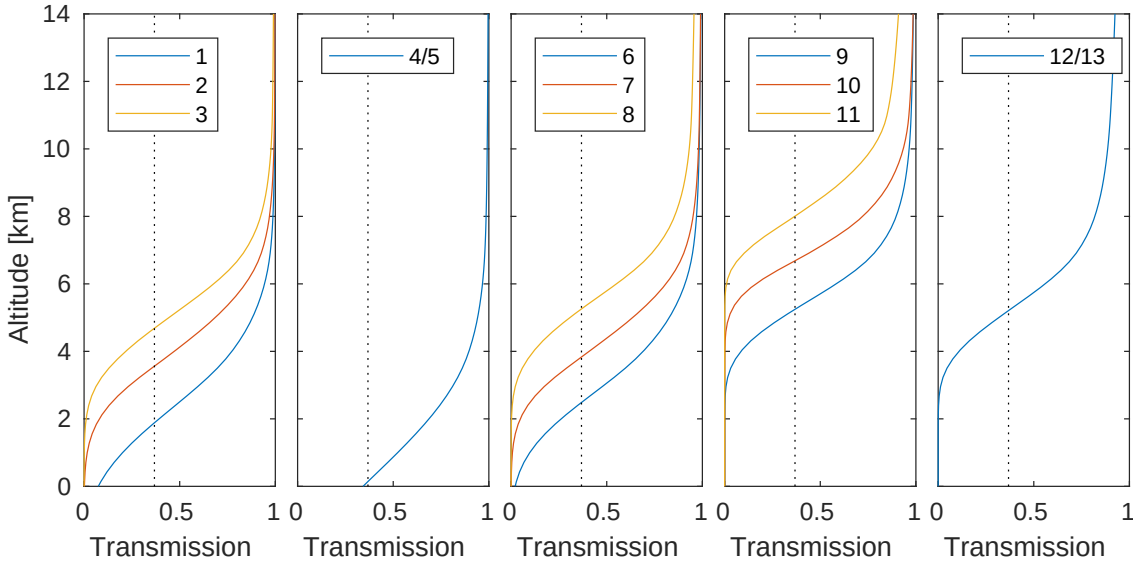

Figure 4. Channel mean transmission between altitudes in the atmosphere and ICI, according to a mid-latitude winter scenario. The dotted line corresponds to an optical thickness of 1.

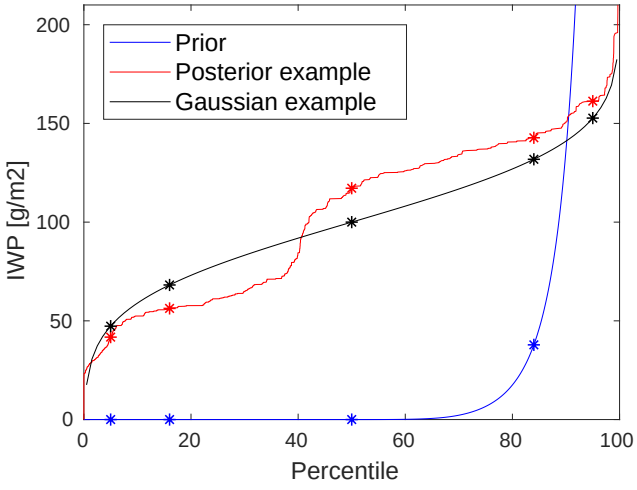

Figure 5. Example quantile functions. The blue line represents the retrieval database applied in Sec. 4.3, acting as prior for a test retrieval (red line). For example, the prior and posterior median values are 0 and 117 $\mathrm{g/m^2}$, respectively. The black line matches a hypothetical retrieval having a Gaussian posterior of $100 \pm 32\,\mathrm{g/m^2}$. The symbol * identifies the 5th, 16th, 50th, 84th and 95th percentiles of each distribution.

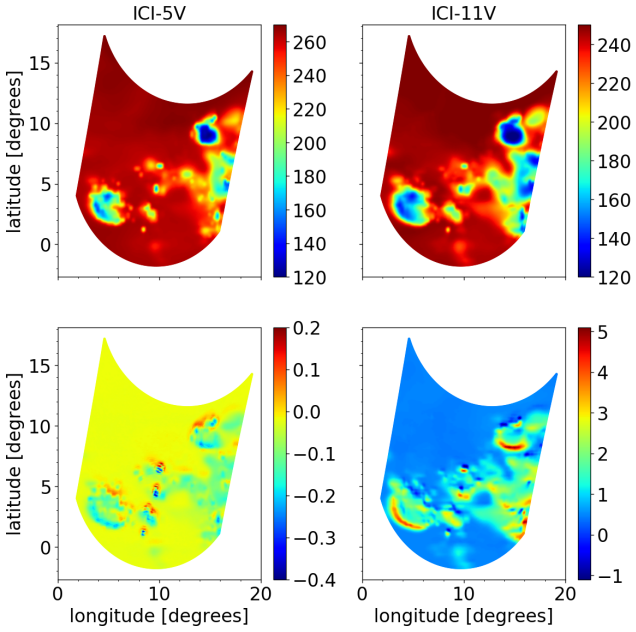

Figure 6. Remapping of ICI-5V and ICI-11V brightness temperatures (K) for an example scene. The upper row shows simulations representing the expected result after remapping (figures showing the data before remapping look identical plotted in this manner). The lower row displays the error found when remapping simulated, noise-free, observations.

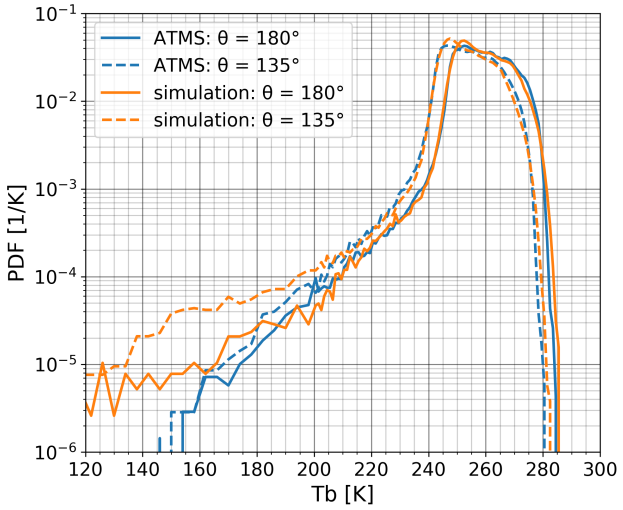

Figure 7. Statistical comparison of simulated and real ATMS channel 21 (183.31±1.8 GHz) measurements, for both a zenith angle of 180° (nadir) and 135° (roughly the one of ICI)~~and~~. Based on data collected between 15°S to 15°N August ~~2015.~~ 2015 (all longitudes included, all ATMS day-time data included, 170 randomly selected CloudSat orbits used).

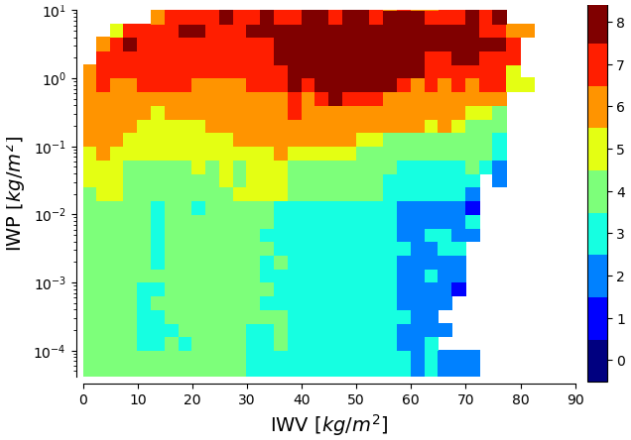

Figure 8. Estimated degrees of freedom (~~DOF~~DoF) of ICI observations, as a function of integrated water vapour (IWV) and IWP. Based on the tropical part of the retrieval database (Sec. 4.3.1).~~Calculated by a singular value decomposition and considering the NEΔT reported in Table 1.~~

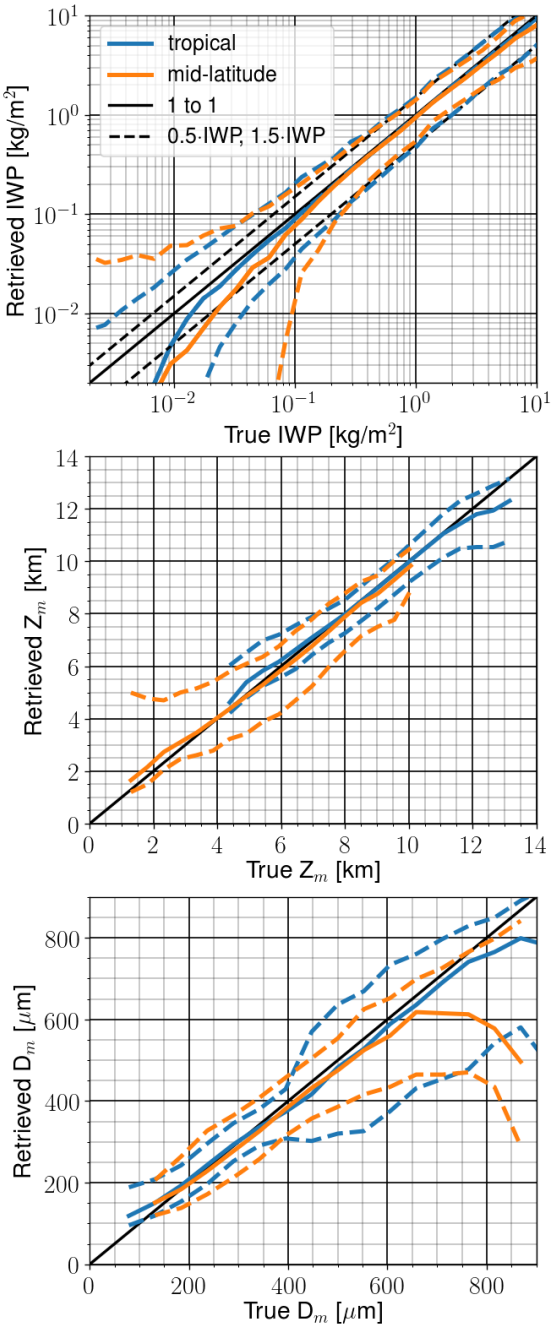

Figure 9. Estimated retrieval performance for IWP (top panel), Z_m (Eq. 4, middle panel) and D_m (Eq. 5, bottom panel). Tropical refers to data at latitudes between 30°S and 30°N, while mid-latitude includes data for November to January ~~and February~~ between 35°–65°N. The blue and yellow solid lines show the median of retrieved median value, while the corresponding dashed lines show the median of retrieved 5th and 95th percentile. The performance for Z_m and D_m is shown for states with an IWP above 25 and 50 $\mathrm{g/m^2}$ for tropical and mid-latitude, respectively.